UPPSALA
UNIVERSITET

Theoretical Studies of Magnetism and Electron Correlation in Solids

OSCAR GRÅNÄS

Dissertation presented at Uppsala University to be publicly examined in Siegbahnsalen, Lägerhyddsv. 1, Uppsala, Tuesday, May 22, 2012 at 10:15 for the degree of Doctor of Philosophy. The examination will be conducted in English.

Abstract
Grånäs, O. 2012. Theoretical Studies of Magnetism and Electron Correlation in Solids. Acta Universitatis Upsaliensis. *Digital Comprehensive Summaries of Uppsala Dissertations from the Faculty of Science and Technology* 920. xii+70 pp. Uppsala. ISBN 978-91-554-8337-1.

This work presents new development and applications of ab-initio simulation tools for material science. Focus lies on materials with strong electronic correlation and strong spin-orbit coupling. Improvements on methods for solving the impurity problem in LDA+DMFT is presented, as well as a reliant method for charge self-consistency in a LMTO based electronic structure code. A new adaptive scheme for Brillouin zone integration is developed, where we show a strong reduction of numerical noise compared to standard techniques. A reformulation of the standard LDA+U method aiming to reduce the number of free parameters is introduced. Fast and realistic reduction of the number of free parameters provides the possibility of high throughput calculations and enabled us to study a large number of compounds. An analysis method for polarization in terms of coupled multipoles, and their corresponding energy contributions is developed and applied. This led to the formulation of Katt's rules, a set of rules complementary to Hund's rules. Katt's rules applies for occupying the orbitals of an electronic shell with strong spin-orbit coupling. The analysis is also used to investigate the unconventional Uranium based superconductors URu_2Si_2, UPt_3, UPd_2Al_3 and UNi_2Al_3, as well as the high temperature superconductor LaOFeAs. We also investigate the non-magnetic delta-phase of Plutonium, providing insight to the electronic structure and the branching ratios of 4d to 5f transitions seen in photo emission spectra.The influence of surface reconstruction on the magneto crystalline anisotropy is investigated in multilayer Fe/ZnSe, showing that Fe deposited on an unreconstructed interface strongly reduces the uniaxial component of the MAE. We provide a detailed understanding of the magnetic properties of Fe_2P, opening possible routes for enhancing the MAE in this system. A general route to strong MAE in nano-laminates is presented, we apply this to propose a candidate with extremely strong anisotropy energy density, $5Fe/2W_{1-x}Re_x$ for x=[0.6-0.8].

Keywords: Magnetism, Superconductivity, Electron Correlation, DMFT, DFT, Actinides, multipoles, hidden order, magnetic anisotropy

Oscar Grånäs, Uppsala University, Department of Physics and Astronomy, Materials Theory, Box 516, SE-751 20 Uppsala, Sweden.

To my family

List of Papers

This thesis is based on the following papers, which are referred to in the text by their Roman numerals.

I   **An LDA+DMFT study of the orbital magnetism and total energy properties of the late transition metals: conserving and non-conserving approximations**
I. di Marco, P. Thunström, O. Grånäs, L. Pourovskii, M. I. Katsnelson, L. Nordström and O. Eriksson
Preprint

II   **Charge self-consistent dynamical mean-field theory based on the full-potential linear muffin-tin orbital method: Methodology and applications**
O. Grånäs, I. di Marco, P. Thunström, L. Nordström, O. Eriksson, T. Björkman and J.M. Wills
Comp. Mat. Sci. 55 pp295 (2012)

III   **Adaptive smearing for Brillouin zone integration**
T. Björkman and O. Grånäs
Int. J. Quantum Chem 111, pp1025-1030 (2011)

IV   **Multipole decomposition of LDA+U energy and its applications to actinide compounds**
F. Bultmark, F. Cricchio, O. Grånäs and L. Nordström
Phys. Rev. B 80 pp035121 (2009)

V   **Analysis of dynamical exchange and correlation in terms of coupled multipoles**
O. Grånäs, I. di Marco, F. Bultmark, F. Cricchio and L. Nordström
Preprint

VI   **Polarisation of an open shell in the presence of spin-orbit coupling**
F. Cricchio, O. Grånäs and L. Nordström
Euro Phys. Lett. 94 pp57009 (2011)

VII   **Multipolar magnetic ordering in actinide dioxides from first-principles calculations**
F. Cricchio, O. Grånäs and L. Nordström
Preprint

VIII   **Itinerant magnetic multipole moments of rank five, triakontadipoles, as the hidden order in URu_2Si_2**

F. Cricchio, F. Bultmark, O. Grånäs and L. Nordström
Phys. Rev. Lett. 103 pp107202 (2009)

IX **Systematic study of the hidden order in URu$_2$Si$_2$ as a multipolar order**
O. Grånäs, F. Cricchio and L. Nordström
Preprint

X **The role of magnetic triakontadipoles in uranium-based superconductor materials**
O. Grånäs, F. Cricchio and L. Nordström
Preprint

XI **Low spin moment due to hidden multipole order from spin-orbital ordering in LaFeAsO**
F. Cricchio, O. Grånäs and L Norström
Phys. Rev. B 81 pp140403(R) (2010)

XII **Microscopic picture of Co clustering in ZnO**
D. Iusan, M. Kabir, O. Grånäs, O. Eriksson and B. Sanyal
Phys. Rev. B 79 pp125202 (2009)

XIII **Assessment of the magnetic properties of SrRuO3 using LDA and LDA+DMFT**
O. Grånäs, I. Di Marco, O. Eriksson, Lars Nordström and C. Etz
Preprint

XIV **Route towards finding large magnetic anisotropy in nanocomposites: Application to a W 1-xRe x/Fe multilayer**
S. Bhandary, O. Grånäs, L. Szunyogh, B. Sanyal, L. Nordström and O. Eriksson
Phys. Rev. B. 84 pp092401 (2011)

XV **On the large magnetic anisotropy of Fe$_2$P**
M. T. J. Costa, O. Grånäs, A. Bergman, P. Venezuela, P. Nordblad, M. Klintenberg and O. Eriksson
Submitted to Phys. Rev. B

XVI **Epitaxial Fe films on ZnSe(001): effect of the substrate surface reconstruction on the magnetic anisotropy**
S. Tacchi, O. Grånäs, A. Stollo, G. Carlotti, G. Gubbiotti, M. Madami, M. Marangolo, M Eddrief, V. H. Etgens, M. K. Yadav, L. Nordström and B. Sanyal
Accepted for publication in J. Phys.: Condensed Matter

Reprints were made with permission from the publishers.

Following papers are co-authored by me, but not included in this thesis

- **Theoretical study of the Mo-Ru sigma phase**
  O. Grånäs, P.A. Korzhavyi, A.E. Kissavos and I.A. Abrikosov
  Calphad (2008) vol. 32 pp. 7

- **A new first principles approach to calculate phonon spectra of disordered alloys**
  O. Grånäs, B. Dutta, S. Ghosh and B. Sanyal
  J. Phys.: Condensed Matter (2011) vol. 24 pp 015402
- **Inhomogeneity in Co doped ZnO diluted magnetic semiconductor**
  B. Sanyal, R. Knut, O. Grånäs, D.M. Iusan and O. Karis
  J Appl Phys (2008) vol. 103
- **Electronic structure of Co doped ZnO: Theory and experiment**
  B. Sanyal, O. Grånäs, R. Knut, V. Coleman, P. Thunström, D.M. Iusan, O. Karis, O. Eriksson and G. Westin
  J Appl Phys (2008) vol. 103
- **Thermodynamics of ordered and disordered phases in the binary Mo-Ru system**
  A.E. Kissavos, S. Shallcross, L. Kaufman, O. Grånäs, A.V. Ruban and I.A. Abrikosov
  Phys Rev B (2007) vol. 75 pp. 184203

Comments on my participation

In the development of the new SPT-FLEX solver I participated in planning the research, running calculations and writing the paper, implementation was done mainly by IdM and PT. The charge self-consistent cycle was implemented jointly by me, IdM, PT, TB and JW. My participation also included planing the research, running calculations, and writing the paper. All parts of the work on the AGS integration scheme were joint between me and TB, with TB doing the main part of the implementation. For the multipole analysis I participated in planing the research, developing the theory and writing the papers. The implementation in the Elk code was done by FC and FB, the implementation in RSPt was done by me. For the work on MAE for nano-laminate I participated in all parts of the work, with SB running more calculations. For the project on Fe$_2$P I contributed with small implementations for analysis, analyzing the results and writing the paper. The work on Fe films on ZnSe is a joint theoretical and experimental work, where I contributed with the main part of the theoretical work, and did not have any part in the experimental work.

Contents

1. Introduction

Magnetism has been important for technological applications for almost a millennia, when the compass was introduced in China [1]. Today we see applications in for example data storage, electrical engines and transformers, to name a few. The main work of this thesis considers magnetism from a computational point of view. Both in terms of methodological development and applications aiming to understand existing materials or design new materials with tailored properties. The purpose of the introductory chapters is to supply the information and basic concepts necessary to understand the research of the published papers. It is in no way self-contained, but includes a number of references to important sources on the topics at hand.

Allready Niels Bohr, in his doctoral thesis [2], and H. J. van Leeuwen in 1921 [3] showed that magnetism can not be described by a classical theory of a moving charged particle, as one might naively think. In this model the net magnetization will always be zero for any electric or temperature field due to the thermal fluctuations. With the introduction of quantum mechanics the intrinsic angular momentum of the electron, *spin*, was included. For ferromagnetic materials the macroscopic magnetic moment originates from the spin of the electron and the orbital angular momentum originating from the electron orbiting the nucleus. The spin magnetic moment associated with the electron is

$$\boldsymbol{\mu}_s = -g\mu_B \frac{\vec{s}}{\hbar} \tag{1.1}$$

where $g \approx 2$ is the electron g-factor, which can be derived from the relativistic description of quantum mechanics. $\vec{s}$ is the quantum mechanical spin operators, given by

$$s_x = \tfrac{\hbar}{2}\sigma_x, \quad s_y = \tfrac{\hbar}{2}\sigma_y, \quad s_z = \tfrac{\hbar}{2}\sigma_z, \tag{1.2}$$

where

$$\sigma_x = \begin{pmatrix} 0 & 1 \\ 1 & 0 \end{pmatrix}, \quad \sigma_y = \begin{pmatrix} 0 & -i \\ i & 0 \end{pmatrix}, \quad \sigma_z = \begin{pmatrix} 1 & 0 \\ 0 & 1 \end{pmatrix} \tag{1.3}$$

are the Pauli matrices, and $\mu_B = \frac{e\hbar}{2mc}$ is the Bohr magneton. The magnetic moment of individual atoms is commonly given in terms of μ_B as the g-factor and the half-integer spin of electron roughly cancels. The orbital magnetic

moment due to the electron orbiting the nucleus is given by

$$\mu_o = -\frac{e}{2mc}(\vec{r} \times \vec{p}) = -\mu_B \vec{l} \qquad (1.4)$$

where $\vec{r}$ is the position of the electron, $\vec{p}$ is the momentum and $\vec{l}$ is the angular momentum. To achieve a net magnetization in a macroscopic sample an imbalance in the occupancy of spin-up and spin-down electrons is needed. However, on a smaller scale a large number of different magnetic orderings can occur. Most of which do not result in a macroscopic net moment, but instead cancels over large length scales. This ordering, however can have effect on a number of macroscopic quantities, like density and thermal expansion (invar effect). The driving mechanism for magnetism is not obvious, at a first glance one might think that the interaction between magnetic dipoles dictates the orientation of the moment. However the energy associated with this interaction is extremely small, and will be overcome by thermal fluctuations even at very low temperature. The most important mechanism is actually the interaction between the electric charge of the electron, together with the anti-symmetric properties associated with all fermions. Further on it will be shown that the Coulomb interaction between the electrons is most cumbersome to treat, part of this thesis is dedicated to how to make an approximate description accurate enough to yield quantitative agreement with measurements, at a reasonable computational cost. For the readers interested in magnetism in the solid state the books by Yoshida[4], Kübler [5] and Mohn [1] are recommended.

2. Theoretical background

This chapter introduces the theoretical background necessary for the continued discussion. The first quantity needed is that which describes the state in which the quantum mechanical system resides. For a many particle system this is the wave function, denoted by $\Psi(\vec{x}_1,\ldots,\vec{x}_n,t)$, where $\vec{x}_i = \vec{r}_i, \vec{s}_i$ is the position vector in real- and spin-space of particle i at time t. Let the particle exchange operator P_{ij} be defined as

$$P_{ij}\Psi(\vec{x}_1,\ldots,\vec{x}_i,\ldots,\vec{x}_j,\ldots,\vec{x}_n,t) = \Psi(\vec{x}_1,\ldots,\vec{x}_j,\ldots,\vec{x}_i,\ldots,\vec{x}_n,t). \quad (2.1)$$

Two successive applications of P_{ij} must lead to the same system, hence $P_{ij}^2 = I$, resulting in two possible characteristics

$$\Psi(\vec{x}_1,\ldots,\vec{x}_i,\ldots,\vec{x}_j,\ldots,\vec{x}_n,t) = \Psi(\vec{x}_1,\ldots,\vec{x}_j,\ldots,\vec{x}_i,\ldots,\vec{x}_n,t) \quad \text{Bosons}$$
$$\Psi(\vec{x}_1,\ldots,\vec{x}_i,\ldots,\vec{x}_j,\ldots,\vec{x}_n,t) = -\Psi(\vec{x}_1,\ldots,\vec{x}_j,\ldots,\vec{x}_i,\ldots,\vec{x}_n,t) \quad \text{Fermions.}$$
$$(2.2)$$

The antisymmetric property of the fermions require that

$$i = j \quad \Rightarrow \quad \Psi(\bar{x},t) = 0 \quad (2.3)$$

which is the Pauli exclusion principle. The time evolution of a non-relativisic system is governed by the Schrödinger equation

$$i\hbar\frac{\partial}{\partial t}\Psi(\vec{x}_1,\ldots,\vec{x}_n,t) = H\Psi(\vec{x}_1,\ldots,\vec{x}_n,t) \quad (2.4)$$

where H is the Hamiltonian, or total energy operator, of the system. In absence of external fields the Hamiltonian has the following form

$$H_S = \sum_I \frac{\vec{p}_I^2}{2M_I} + \sum_i \frac{\vec{p}_i^2}{2m_e} + \frac{1}{2}\sum_{I,J}\frac{Z_I Z_J e^2}{|\vec{R}_I - \vec{R}_J|} + \frac{1}{2}\sum_{i,j}\frac{e^2}{|\vec{r}_i - \vec{r}_j|} - \sum_{I,i}\frac{Z_I e^2}{|\vec{R}_I - \vec{r}_i|} \quad (2.5)$$

where M_I, Z_I and R_I refer to the mass, number of protons and the position of nuclei I, m_e and r_i are the mass and position of an electron. From left the terms describe the kinetic energy of the nuclei, the kinetic energy of the electrons, the electrostatic energy between the nuclei, the electrostatic energy between the electrons and the electrostatic energy between the nuclei and electrons. As there is no explicit time dependence in Eq. 2.5 the spatial and time dependence of the wave function can be separated. If the spatial part is expressed in an

eigen basis to H, with $\Psi(\vec{x}_i, t) = \psi_E(\vec{x}_i)e^{-\frac{iEt}{\hbar}}$ eq. 2.4 reduces to

$$H\Psi = E\Psi \tag{2.6}$$

where E is the energy of the system. That is, no energy is dissipating from the system. The state with the lowest energy, the ground state, can be found through a variational procedure following the Euler-Lagrange equations.

2.1 Born-Oppenheimer approximation

In reality the atoms are not stationary, which will complicate our picture slightly. It would be very convenient if we could separate the motion of the electrons from the motion of the nuclei. For a system where this could be done we can write the electronic wave function as

$$\Psi(\vec{R}_I, \vec{r}_i) = \psi(\vec{R}_I, \vec{r}_i)\phi(\vec{R}_I) \tag{2.7}$$

with the demand that $\psi(\vec{R}_I, \vec{r}_i)$ is the solution to the electronic part of the Schrödinger equation with the positions of the nuclei $\vec{R}_I$ fixed, i.e.

$$
\begin{aligned}
H_{Se}\psi &= \left(\sum_i \frac{\vec{p}_i^2}{2m_e} + \frac{1}{2}\sum_{i,j} \frac{e^2}{|\vec{r}_i - \vec{r}_j|} - \sum_{I,i} \frac{Z_I e^2}{|\vec{R}_I - \vec{r}_i|}\right)\psi = \\
&\left(\sum_i \frac{\vec{p}_i^2}{2m_e} + \frac{1}{2}\sum_{i,j} \frac{e^2}{|\vec{r}_i - \vec{r}_j|} + V(\vec{r}_i)\right)\psi = E_e\psi.
\end{aligned}
\tag{2.8}
$$

Applying the Hamiltonian to the full wave function results in

$$
\begin{aligned}
H_S\Psi &= \left(\sum_I \frac{\vec{p}_I^2}{2M_I} + \frac{1}{2}\sum_{I,J} \frac{Z_I Z_J e^2}{|\vec{R}_I - \vec{R}_J|} + \sum_i \frac{\vec{p}_i^2}{2m_e} + \frac{1}{2}\sum_{i,j} \frac{e^2}{|\vec{r}_i - \vec{r}_j|} - \sum_{I,i} \frac{Z_I e^2}{|\vec{R}_I - \vec{r}_i|}\right)\Psi \\
&= \psi\left(\sum_I \frac{\vec{p}_I^2}{2M_I} + \frac{1}{2}\sum_{I,J} \frac{Z_I Z_J e^2}{|\vec{R}_I - \vec{R}_J|} + E_e(\{\vec{R}_I\}) - \sum_{I,i} \frac{Z_I e^2}{|\vec{R}_I - \vec{r}_i|}\right)\phi \\
&\quad - \sum_I \frac{1}{2M_I}\left(2\vec{p}_I\phi\vec{p}_I\psi + \phi\vec{p}_I^2\psi\right).
\end{aligned}
\tag{2.9}
$$

From this it is clear that if the last two terms are ignored, the equations can be solved for the electrons and nuclei separately, by making $\phi(\vec{r})$ satisfy

$$\left(\sum_I \frac{\vec{p}_I^2}{2M_I} + \frac{1}{2}\sum_{I,J} \frac{Z_I Z_J e^2}{|\vec{R}_I - \vec{R}_J|} + E_e(\{\vec{R}_I\}) - \sum_{I,i} \frac{Z_I e^2}{|\vec{R}_I - \vec{r}_i|}\right)\phi = E_n\phi \tag{2.10}$$

This approximation is known as the Born-Oppenheimer- (BO), or adiabatic approximation [6] , it assumes that the electrons do not change eigenstates as the nuclei move. This is often a good approximation as the electrons are much lighter than the nuclei and therefore move much faster, they can adjust to the new position of the nuclei very fast and see it as a stationary electric field, cases when BO is not valid is for example BCS superconductivity. From now on we will only consider the electronic part of the Hamiltonian.

2.2 Crystals and the Bloch theorem

The basic equations describing the electronic system is known, yet unsolvable in its current form. The main problem is that the set of equations is enormous for any macroscopic sample, with a particle number in the order of Avogadro's number, $\sim 10^{23}$. For solids in a crystalline phase there is a theorem by F. Bloch[7] dating back to 1929, for one-dimensional solids this was realized already in 1883 by G. Flouquet [8], that reduces the complexity using the periodicity of the crystal as argument. Due to the periodic arrangement of the nuclei the electrons experience a periodic potential from the electric charge of the nuclei. A crystal is made up of a Bravais lattice and a basis. The basis is just the positions of the atoms in the primitive cell, the Bravais lattice is all points conected by the vector $\vec{R} = n_1\vec{a}_1 + n_2\vec{a}_2 + n_3\vec{a}_3$, where $\vec{a}_i$ is a lattice vector and n_i is an integer. The Bloch theorem now states that the eigenstates ψ the Hamiltonian, where $V(\vec{r}) = V(\vec{r}+\vec{R})$ is a periodic potential, and $\vec{R}$ is any Bravais lattice vector, can be expressed as a plane wave times a periodic function $u_{n\vec{k}}(\vec{r}) = u_{n\vec{k}}(\vec{r}+\vec{R})$, i.e.

$$\psi_{n\vec{k}}(\vec{r}) = e^{i\vec{k}\cdot\vec{r}} u_{n\vec{k}}(\vec{r}) \tag{2.11}$$

where n is the band index and $\vec{k}$ the wave number. That is, bulk properties can now be calculated using only one primitive cell. This simplifies things enormously, since most crystal structures can be represented by only a few atoms. In a real sample surface atoms are naturally present, luckily they make up about $N^{2/3}$ of the total number of atoms N. That means about 1 out of 10^8 atoms are at the surface, hence this approximation is often good. The primitive cell of the crystal is not only determined by the time averaged position of the ions, for example magnetic ordering can reduce the symmetry. If lattice vibrations are considered the cell is increased to the point where all phonon q-vectors under consideration are encompassed in the cell.

2.3 Relativistic description

In many cases the Schrödinger equation gives an inadequate description of solids, particularly when magnetism is included. The Schrödinger equation (eq 2.4) has no explicit dependence on spin, and therefore contains no coupling between spin space and real space, something that is known to be important for e.g. the magneto-crystalline anisotropy (the classical dipole-dipole interaction is extremely small for highly symmetric bulk crystals). A more elaborate treatment is described by the so-called Dirac equation, a relativistic counterpart of the Schrödinger equation incorporating also the anti particles. The wave function in the relativistic formulation is then a four-component

spinor, one two-component for the electron and one for the positron.

$$|\Psi\rangle = \left[\begin{array}{c} |\Psi^e\rangle \\ |\Psi^p\rangle \end{array} \right] \quad (2.12)$$

The Hamiltonian in this has has the form

$$H = \left[\begin{array}{cc} V(\vec{r}) + mc^2 & c\vec{\sigma} \cdot \vec{p} \\ c\vec{\sigma} \cdot \vec{p} & V(\vec{r}) + mc^2 \end{array} \right]. \quad (2.13)$$

Assuming $H|\Psi\rangle = E\Psi\rangle$ the electronic part of the eigenvalue equation becomes

$$[-E - mc^2 - V(\vec{r})) + c^2(\vec{\sigma} \cdot \vec{p})(E + mc^2 - V(\vec{r}))^{-1}(\vec{\sigma} \cdot \vec{p})]|\Psi^e\rangle = 0 \quad (2.14)$$

where $\vec{p}$ is the momentum, c is the speed of light. We can now see that spin and orbital space couple through the $c\vec{\sigma} \cdot \vec{p}$ terms. For the solids studied in this thesis we do not need the treatment of the anti-particles, and will therefore reduce the equations to the non-relativistic limit, considering an atom-like central potential [9]. The resulting Hamiltonian contains the terms from eq. 2.5 with some additional terms.

$$H = H_{\mathrm{Se}} - \sum_i \frac{\vec{p}_i^4}{8m_e^3 c^2} + \frac{\hbar^2}{8m_e^2 c^2}\nabla^2 V(\vec{r}) - \frac{1}{2m^2 c^2}\frac{1}{r}\frac{dV}{dr}\sum_i \vec{l}_i \cdot \vec{s}_i. \quad (2.15)$$

The first added term is the mass-velocity term, a correction to the kinetic energy. The second is the Darwin term, a correction to the potential. The last term is the spin-orbit coupling, the pre factor $\xi = \frac{1}{r}\frac{dV}{dr}$ is commonly called the spin-orbit coupling constant. With the inclusion of the spin-orbit interaction we have an explicit coupling between the spin and orbital degrees of freedom. This is quite weak for light elements, but as the number of protons in the nucleus increases, the spin-orbit coupling constant is enhanced. For example in actinide compounds it is sometimes considerably larger than the level splitting from the crystal electric field.

3. Many-particle physics and approximations

From now on all equations will be in Rydberg atomic units, i.e. $\hbar = 2m_e = e^2/2 = 1$, henceforth reserving the letter e for the exponential function. The Hamiltonian in eq. 2.8 is still intractable for most systems, the problem lies in the $\sum_{i,j} \frac{1}{|\vec{r}_i - \vec{r}_j|}$ term which couples the movement of one electron to all other electrons in the system, i.e. the electrons are *correlated*. For example, the electronic repulsion will lead to a suppressed electron density in the vicinity of an electron, called *exchange correlation hole*. If we would like to calculate the ground state of the system we would have to set up a basis consisting of all possible states, something that is computationally impossible for almost all systems with todays techniques. Hence approximations are needed, a common approach is to construct a so called *mean field*, taking into account correlations on an average only, expressing the other electrons as an effective potential. This leads to a single particle problem, which in turn may be solved taking into account temperature only through the Fermi-Dirac distribution. Another approach is to map the part of the problem which is strongly correlated to a reduced problem possible to solve including the proper correlation effects, hybridizing with the environment through a mean field.

3.1 The Hartree-Fock approximation

Based on the antisymmetric properties of the wave function a set of equations is derived forming an effective single-particle problem, the equations are generally known as the Hartree-Fock (HF) equations. It might be tempting to construct the many-particle wave function as a product of single particle wave functions, $|\Psi\rangle = \Pi_i \psi_i(\vec{x}_i)$, however the anti-symmetric properties will not be obeyed, hence the Pauli exclusion principle eq. 2.3 will not be satisfied and this type of wave function is of no use for fermionic systems. However, Slater noted that the properties of the determinant makes it suitable as a basis [10],

introducing the so called *Slater determinant*

$$|\Psi\rangle = \frac{1}{\sqrt{N!}} \begin{vmatrix} \psi_1(\vec{x}_1) & \psi_1(\vec{x}_2) & \ldots & \psi_1(\vec{x}_n) \\ \psi_2(\vec{x}_1) & \ddots & & \vdots \\ \vdots & & & \\ \psi_n(\vec{x}_1) & & \ldots & \psi_n(\vec{x}_n). \end{vmatrix} \qquad (3.1)$$

Proceeding to minimize the energy of the Hamiltonian in eq. 2.8 following the Euler-Lagrange procedure results in the following Schrödinger-like equation

$$\begin{aligned} &\left(-\vec{p}^2 + V(\vec{r})\right)\psi_i(\vec{x}) \\ &+ \sum_j \int d\vec{r}d\vec{r}' \, \psi_j^*(\vec{x}')\psi_j(\vec{x}')\frac{1}{|\vec{r}-\vec{r}'|}\psi_i(\vec{x}) \\ &- \sum_j \int d\vec{r}d\vec{r}' \, \psi_j^*(\vec{x}')\psi_i(\vec{x}')\frac{1}{|\vec{r}-\vec{r}'|}\psi_j(\vec{x})\delta_{s_i,s_j} = \varepsilon_i\psi_i(\vec{x}) \end{aligned} \qquad (3.2)$$

Now two potential terms originating from the electron-electron interaction can be identified, the first one being

$$V_i^{\text{h}}(\vec{r}) = \sum_{j\neq i} \int d\vec{r}' \, \psi_j^*(\vec{x}')\psi_j(\vec{x}')\frac{1}{|\vec{r}-\vec{r}'|} \qquad (3.3)$$

is the so called Hartree term, an effect of the Coulomb interaction between the electron and the charge distribution of all other electrons. The other term is non-local and acts only on parallel spins due to its quantum mechanical origin,

$$V_i^{\text{x}}(\vec{r},\vec{r}') = -\sum_{j\neq i} \delta_{\vec{s},\vec{s}'} \psi_j^*(\vec{x}')\psi_i(\vec{x})\frac{1}{|\vec{r}-\vec{r}'|}, \qquad (3.4)$$

known as the exchange potential. As the exchange potential acts only on parallel spins different potential for spin up and down, This can in turn lead to spontaneous symmetry breaking and magnetism. Later the term *correlation energy* will be used, according to quantum chemistry defined as the difference from the HF energy compared to the results of a more rigorous treatment of the electrostatic interaction between the electrons. In this thesis we will also use the term *screened exchange* for a Hartree-Fock like static potential with an artificially screened Coulomb interaction. The HF approximation suffers from a variety of problems due to it's mean field nature, most severe is that it lacks the correlation hole. This has two implications, first there is a binding force between the electron and the correlation hole due to the positive charge of the hole. Secondly the correlation hole screens the charge of the electron, and therefore the interaction between neighboring electrons are weakened. In the HF approximation this is not taken into account, hence the interaction strength is overestimated, HF does however perform reasonably well for systems with

a small number of electrons, where many body effects are not so important, e.g. when applied to small molecules.

3.2 Density functional theory

An alternative approach to the orbital based techniques, such as the Hartree-Fock approximation, are the density functional theories (DFT). In DFT the many-body problem is circumvented by working with the density instead of the wave function. Only a brief presentation is made, excellent reviews on the subject are Dreizler and Gross [11], Capelle [12] and Burke [13]. The development of density functional theory boosted significantly with the proof of Hohenberg and Kohn [14], stating that the ground state electron density is enough to completely determined the Hamiltonian, and therefore all properties, or more exactly:

Theorem 1 *For any system of interacting particles in an external potential $V_{ext}(\vec{r})$, the potential $V_{ext}(\vec{r})$ is determined uniquely, up to a constant shift, by the ground state density $n_0(\vec{r})$.*

Theorem 2 *A universal functional for the energy $E[n]$ in terms of the density $n(\vec{r})$ can be defined, valid for any external potential $V_{ext}(\vec{r})$. For any particular $V_{ext}(\vec{r})$, the exact ground state energy of the system is the global minimum value of this functional, and the density $n(\vec{r})$ that minimizes the functional is the exact ground state density $n_0(\vec{r})$.*

The proofs is not discussed in this thesis, interested readers are referred to the recommended literature, details regarding for example *v*-representability is also excluded as they are to a large extent overcome by the Levy constrained search method [15, 16]. This means in principle that since the Hamiltonian is fully determined by $V_{ext}(\vec{r})$, which in turn is uniquely determined by $n_0(\vec{r})$, the only quantity needed for a full description of the ground state is the density. To determine the ground state density only the functional $E[n]$ is needed, unfortunately the theorems provide no means of finding $E[n]$, hence approximate functionals are developed.

3.2.1 Kohn-Sham equations

Kohn and Sham proposed a scheme how to use DFT in practice [17]. Using variational calculus they derived a Schrödinger like single particle equation similar to the Hartree-Fock equations[1]. The scheme is based on the assumption that you can find a system of fictitious non-interacting quasi particles,

---

[1]Earlier approaches, such as the Thomas-Fermi approximation, describes all terms in the Hamiltonian as a functional of the density. These methods has some applicability at very high pressures, but often fails as a result of a large error in the kinetic energy.

with the same density as a system of electrons. The quasi particles are non-interacting, hence we work in a single particle basis. The orbitals, denoted $\psi_i(\vec{r})$, fulfill the equations

$$H^{\text{eff}}\psi_i(\vec{r}) = \left(T + V_s^{\text{eff}}\right)\psi_i(\vec{r}) = \varepsilon_i\psi_i(\vec{r}) \tag{3.5}$$

and

$$n(\vec{r}) = \sum_{i \in \text{occ}} |\psi_i(\vec{r})|^2 \tag{3.6}$$

where the V_s^{eff} is the effective single particle potential. As we assume that the density minimizes the energy it should also satisfy the Euler Lagrange equation

$$\frac{\delta T_s[n]}{\delta n(\vec{r})} + V_s^{\text{eff}}(\vec{r}) = \mu \tag{3.7}$$

where $T_s[n]$ is the minimum kinetic energy and μ is the chemical potential. V_s^{eff} is the effective potential of the single particle, it is defined as

$$V_s^{\text{eff}} = V^{\text{ext}} + \frac{\delta E^{\text{h}}}{\delta n(\vec{r})} + \frac{\delta E^{\text{xc}}}{\delta n(\vec{r})} \tag{3.8}$$

where the energy E^{xc} includes both exchange and correlation, in contrast to the E^{x} appearing in the Hartree Fock expression. The minimum kinetic energy is defined by

$$T_s[n] = \min_{\Psi \to n} \langle\Psi|\sum_{i \in \text{occ}}\vec{p}_i|\Psi\rangle, \tag{3.9}$$

which in practice is often calculated by

$$T_s[n] = \sum_{i \in \text{occ}} \varepsilon_i - \int d\vec{r}V_s^{\text{eff}}n(\vec{r}), \tag{3.10}$$

to avoid calculating gradients of the wave function. We can now construct the total energy from this non-interacting kinetic energy

$$E[n] = T_s[n] + E^h[n] + E^{\text{xc}}[n] + \int d\vec{r}V^{\text{ext}}(\vec{r})n(\vec{r}). \tag{3.11}$$

According to Hohenberg and Kohn's theorems all ground state properties should be available from the density, but due to technical reasons it is problematic to calculate magnetic properties from just the charge density. To circumvent this the formalism is extended to include also the magnetization density $\vec{m}(\vec{r})$, i.e. spin-density functional theory (SDFT). This formalism was developed in 1972 by Von Barth and Hedin [18].The argument for validity is very similar to the one for DFT, two different non-degenerate ground states will

always lead to different charge $n(\vec{r})$ and magnetization densities $\vec{m}(\vec{r})$. Since the spin-operators in eq. 1.2 are described by 2×2 matrices, the approach is to represent the density and effective potential in this form as well.

$$
\begin{aligned}
n(\vec{r}) &\Rightarrow \rho(\vec{r}) = \begin{pmatrix} \rho_{\alpha\alpha}(\vec{r}) & \rho_{\alpha\beta}(\vec{r}) \\ \rho_{\beta\alpha}(\vec{r}) & \rho_{\beta\beta}(\vec{r}) \end{pmatrix} \\
V_s^{\text{eff}}(\vec{r}) &\Rightarrow \vec{V}_s^{\text{eff}}(\vec{r}) = \begin{pmatrix} V_{\alpha\alpha}(\vec{r}) & V_{\alpha\beta}(\vec{r}) \\ V_{\beta\alpha}(\vec{r}) & V_{\beta\beta}(\vec{r}) \end{pmatrix}.
\end{aligned}
\tag{3.12}
$$

The wave functions will be represented as two-component spinors

$$
\psi_i(\vec{r}) \quad \Rightarrow \quad \psi_i(\vec{r}, \vec{s}) = \psi_i(\vec{x}) = \begin{pmatrix} \psi_{i\alpha}(\vec{r}) \\ \psi_{i\beta}(\vec{r}) \end{pmatrix}
\tag{3.13}
$$

following eq. 3.6 we write the density matrix as

$$
\rho(\vec{r}) = \sum_{i \in \text{occ}} \begin{pmatrix} |\psi_{i\alpha}(\vec{r})|^2 & \langle \psi_{i\alpha}(\vec{r}) | \psi_{i\beta}(\vec{r}) \rangle \\ \langle \psi_{i\beta}(\vec{r}) | \psi_{i\alpha}(\vec{r}) \rangle & |\psi_{i\beta}(\vec{r})|^2 \end{pmatrix}
\tag{3.14}
$$

which is generally expanded in terms of the charge and magnetization densities

$$
\rho(\vec{r}) = \frac{1}{2} [n(\vec{r}) + \vec{m}(\vec{r}) \cdot \vec{\sigma}].
\tag{3.15}
$$

By using the variational principle we get the following magnetic Kohn-Sham equation

$$
\sum_{\beta} \left(T \delta_{\alpha,\beta} + V_{s\alpha\beta}^{\text{eff}} \right) \psi_{i\beta}(\vec{r}) = \sum_{\beta} \varepsilon_i \delta_{\alpha,\beta} \psi_i(\vec{r})
\tag{3.16}
$$

with

$$
V_{\alpha\beta}^{\text{eff}} = V_{\alpha\beta}^{\text{ext}} + \frac{\delta E^{\text{h}}}{\delta n(\vec{r})} + \frac{\delta E^{\text{xc}}[\rho]}{\delta \rho_{\beta\alpha}(\vec{r})}
\tag{3.17}
$$

we still have to determine the functional $E^{\text{xc}}[n]$, that is, a functional of the density which gives the proper exchange and correlation energy.

3.2.2 Exchange and correlation

The exchange correlation energy consists of two parts, exchange and correlation, $E^{\text{xc}} = E^{\text{x}} + E^{\text{c}}$. There are many ways of approximating E^{xc}, it is most tractable in terms of computational speed if one can find a functional which is local. For the classes of local approximations we can write the exchange

correlation energy simply as a function of the density

$$E^{xc}[n(\vec{r})] = \int d\vec{r}\varepsilon(n(\vec{r})) \qquad (3.18)$$

The exchange energy in DFT is defined by

$$E^{x}[n] = \langle \Psi[n]|V^{e-e}|\Psi[n]\rangle - V^{h}[n] \qquad (3.19)$$

i.e. the electron-electron interaction evaluated of the Kohn-Sham orbitals excluding the Hartree term. The correlation part is now defined as the remainder, unknown energy

$$E^{c}[n] = E[n] - T_{s}[n] - E^{h}[n] - E^{x}[n] \qquad (3.20)$$

hence, the difference in the true energy to that of the terms already incorporated. In the so called Local Density Approximation (LDA) $E^{x}[n]$ and $E^{c}[n]$ is determined from very accurate Monte Carlo simulations of the homogeneous electron gas in different densities. These are later parametrized to an easy accessible form, for $E^{c}[n]$ several parameterizations are available, originally Wigner correlation was used, later Ceperley and Alder [19], Vosko,Wilk and Nussair [20], von Barth and Hedin [18], Perdew and Zunger [21], among others provided parameterizations with different features. Extensions to include gradients to the electron density in the functional is also common, they are denoted Generalized Gradient Approximations (GGA's) [22, 23, 24]. DFT has proven very successful over the years, and has proven transferability for large parts of the periodic system, even though the exchange-correlation functionals are approximate. It is argued that this is due to simple physical properties conserved by the functionals, for example the exchange hole integrates to 1, and the correlation hole to zero. However, for systems with very localized states, like transition metal oxides and f-electron systems the LDA/GGA schemes are inadequate. This is due to non-local effects, hence the explicit Coulomb interaction has to be taken into account to some approximation.

3.2.3 LDA+U

One scheme to incorporate explicit Coulomb interaction between some orbitals is to use a HF like approach for the states which are localized [25]. This is realized by not using only the density, but the density matrix, to calculate interactions between electrons. It generally known as DFT+U or LDA+U scheme, where U is the Coulomb interaction term. It is similar to HF in the sense that the energy and potential is expressed in the same way, however, it is the Kohn-Sham orbitals from DFT that supply the basis, not the variational orbitals resulting from the energy minimization in the HF model. The LDA+U Hamiltonian is characterized by the standard DFT Hamiltonian, plus an extra term added only for a set of correlated orbitals $\{\psi_{\vec{R},\xi_i}(\vec{x})\} = \{|\vec{R},\xi_i\rangle\}$ centered

on cite $\vec{R}$,

$$H_{\text{LDA}+U} = H_0 + H_U = H_{\text{LDA}} + \frac{1}{2} \sum_{\vec{R},\xi_1,\xi_2,\xi_3,\xi_4 \in L_U} U_{\xi_1\xi_2\xi_3\xi_4} c^\dagger_{\vec{R},\xi_1} c^\dagger_{\vec{R},\xi_2} c_{\vec{R},\xi_3} c_{\vec{R},\xi_4}$$

(3.21)

where the L_U denotes the correlated subspace, i.e. orbital and spin index, and H_{LDA} is the effective LDA Hamiltonian of eq. 3.5. The U-matrix is defined by

$$U_{\xi_1\xi_2\xi_3\xi_4} = \int d\vec{x} d\vec{x}' \, \psi^\dagger_{\vec{R},\xi_1}(\vec{x}) \psi^\dagger_{\vec{R},\xi_2}(\vec{x}') g(\vec{r}-\vec{r}') \psi_{\vec{R},\xi_3}(\vec{x}) \psi_{\vec{R},\xi_4}(\vec{x}') \qquad (3.22)$$

Using the density matrix in eq. 3.14 we write the most general expression for the HF-like energy as

$$E^U = \frac{1}{2} \sum_{\xi_1\xi_2\xi_3\xi_4} \left[\rho_{\xi_1\xi_3}\rho_{\xi_2\xi_4} - \rho_{\xi_1\xi_4}\rho_{\xi_2\xi_3} \right] U_{\xi_1\xi_2\xi_3\xi_4} \qquad (3.23)$$

where $g(\vec{r}-\vec{r}')$ is the interaction. It might be tempting to use the Coulomb interaction $g = \frac{1}{\vec{r}-\vec{r}'}$, like in the HF approximation. However since the HF approximation is free of screening effects this energy is largely overestimated. Instead one uses a reduced value, where the reduced interaction strength can be determined from a number of schemes e.g. constrained LDA [26, 27] and constrained RPA [28], but in practice often determined by varying the strength and comparing some physical quantities to experiment.

3.3 Dynamic mean field theory

A more rigorous method to treat electronic systems is the so-called Spectral Density Functional Theory (SDFT). Here the central quantity is the energy dependent spectral density, instead of the energy independent electron density from DFT. The energy dependence of SDFT captures the full excitation spectra of the electronic system, hence the exchange and correlation has to be treated explicitly. A full solution to the SDFT problem is still beyond the possibility of todays computers. However, for some model Hamiltonians the machinery to deal with *local* correlation effects, including many body effects, is well developed. In the Anderson impurity model (AIM) [29] the approach is to consider highly localized electrons in a host of itinerant electrons. The localized electrons are allowed to interact with the host through a hybridization term and with each other with the Coulomb interaction U. For another category of model Hamiltonians, lattice models, one originally had two limits with easily accessible solutions, the $U/W = \infty$ and the $U/W = 0$, where W denotes the band width of the valence electrons. A different limit originates from 1989 when Metzner and Vollhardt [30] descovered that diagrammatic treatment of the electron correlation is greatly simplified in infinite dimen-

sions $d \to \infty$. It was followed by Georges and Kotliar in 1992[31] who proved that the so called Hubbard model can be mapped onto the AIM, and that the mapping becomes exact in infinite dimensions. The machinery is referred to as Dynamical Mean Field Theory (DMFT), and allows for mapping lattice models, in particular the Hubbard model, to the single impurity AIM,

$$
\begin{aligned}
H_{\text{AIM}} = &\sum_{ij} \varepsilon_{ij} c_i^\dagger c_j + \frac{1}{2} \sum_{i,j,k,l} U_{ijkl} c_i^\dagger c_j^\dagger c_k c_l \\
&+ \sum_{kij} V_{k,ij}^\dagger (c_i^\dagger s_{k,j} + s_{k,i}^\dagger c_j) + \sum_{k,i} \varepsilon_{k,i} s_{k,i}^\dagger s_{k,i}
\end{aligned}
\tag{3.24}
$$

where c represents correlated electrons and s free electrons. The DMFT is an approximation to and exact SDFT, just as LDA is an approximation to the exact exchange correlation functional in DFT. Anisimov, Poteryaev *et. al.* [32] and Lichtenstein and Katsnelson [33] realized how this scheme can be used to map the LDA+U Hamiltonian in eq. 3.21 on an impurity model much like the AIM, leaving weakly correlated electrons to LDA, and strongly correlated to an *impurity solver* of choice. The Coulomb interaction between the correlated electrons in the impurity are described by a self-energy $\Sigma_{\vec{R}}(i\omega_n)$, whereas the Coulomb interaction between weakly correlated electrons, and between impurity and weakly correlated electrons are described with LDA. Self-consistency is reached when the local Green's function is unchanged from the previous iteration, i.e. the self-energy and the chemical potential μ is conserved according to Fig 4.2. The self-energy in the correlated subspace is determined by the bath Green's-function

$$
\widehat{\mathcal{G}}_{0,\vec{R}}(i\omega_n) = [(i\omega_n + \mu)\widehat{1} - \widehat{\mathcal{H}}_{0,\vec{R}} - \widehat{\Delta}(i\omega_n)]^{-1}
\tag{3.25}
$$

The resulting self-energy is then projected back to the LDA basis and the full Green's-function

$$
\widehat{G}_{\vec{k}}(i\omega_n) = [(i\omega_n + \mu)\widehat{1} - \widehat{H}_{\vec{k}}^{LDA} - \sum_{\vec{R}} \widehat{\Sigma}_{\vec{R}}(i\omega_n)]^{-1}
\tag{3.26}
$$

The procedure of projecting to the correlated basis, and embedding the resulting self-energy into the LDA basis set, will be presented in more detail in chapter 4, and Paper II. A number of good reviews exist, the interested reader is referred to [34, 35, 36, 37, 38]. A variety of impurity solvers exist for the AIM, and many are generalized to the multi-orbital case, and applicable in the LDA+DMFT framework. The impurity solvers can be classified into three main categories: the ones treating hybridization exactly and approximates the Coulomb interaction, the ones treating Coulomb interaction exactly and approximates the hybridization, and formally exact quantum Monte-Carlo (QMC) solvers. QMC is not used in any research presented in this thesis due to its time consuming nature, hence a more detailed description is omitted.

The two main branches of QMC used in LDA+DMFT is the Hirsh-Fye(HF) QMC[39, 40] and the continuous time(CT) QMC[41], where the CT-QMC currently seems to be the better choice. The QMC family of solvers are able to resolve the metal-insulator transition, i.e. they are reliable for arbitrary correlation strength U/W, but the computational cost is high and analytical continuation of the self-energy to real energy has some extra difficulties due to numerical noise. Care has to be taken as the Coulomb interaction on the impurity is taken into account twice, once in LDA and once in the impurity solver, this is solved by including a *double counting* (DC) term.

3.3.1 Solvers with approximate Coulomb interaction

This set of solvers generally work with a perturbation expansion in the Coulomb interaction. With only the lowest order terms included, i.e. the Hartree and Fock terms, the LDA+U method is recovered. This is a static approximation and DMFT is in principle not needed, but implementation is trivial and easy to test due to the large number of published results using LDA+U. For lattice models, Bickers and Scalapino[42] proposed the so called fluctuation exchange (FLEX) approximation, describing interaction between quasi particles with collective pair-, spin-, and charge fluctuations. This was first used for realistic problems by Lichtenstein and Katsnelson who calculated mainly magnetic properties of transition metals [33, 43]. FLEX was later generalized to include also spin-orbit interaction (i.e. the spin-flip terms) by Pourovskii *et. al.* [44], introducing Spin-polarized T-matrix Fluctuation Exchange (SPT-FLEX) approximation, this has proven to be a reliable method for itinerant actinides and actinide compounds [45, 46, 47]. When it comes to spectral properties this category of solvers works either for strong correlation, $U/W >> 1$ (LDA+U) or weak to moderate correlation far from phase transitions, $U/W < 1$ (FLEX, SPT-FLEX), in general they are not able to catch the metal insulator transition.

3.3.2 Summary of Paper I: Improvements on the SPT-FLEX solver

In this work we propose an alternative scheme for the FLEX family of solvers. Our work is based on the SPT-FLEX, but our proposed improvements are applicable also for basic FLEX. The original FLEX obeys the conservation laws for particle number, momentum and energy from Kadanoff and Baym[48]. Simply put, T-matrix takes into account inter-particle collisions, which are excluded in the HF approximation. The T-matrix is expressed through the ladder diagrams and results in a Dyson-like equation. The self-energy is constructed in similar manner to the random-phase approximation, however, the bare Coulomb interaction is substituted for the static part of the T-matrix, which will include screening for the particle-particle (PP) and particle-hole

(PH) channels. A few choices can be made in the diagrammatic expansion. First of all which channels are important, where we have adopted the main features of Drchal et. al [49], depicted in Fig. 3.1. There is also an option to choose different propagators between the scattering events, traditionally one uses the unperturbed local Green's function

$$\mathscr{G}_0(i\omega_n) = [(i\omega_n + \mu) - \mathscr{H}_0 - \Delta(i\omega_n)]^{-1} \quad (3.27)$$

or the full local Green's function

$$\mathscr{G}(i\omega_n) = [(i\omega_n + \mu) - \mathscr{H}_{0,\vec{R}} - \Delta(i\omega_n) - \Sigma(i\omega_n)]^{-1}. \quad (3.28)$$

To obey thermodynamic conservation laws the self-energy has to be generated from the full local Green's function, i.e.

$$\widehat{\Sigma}[\mathscr{G}] = \frac{\delta\Phi[\mathscr{G}]}{\delta\mathscr{G}}, \quad (3.29)$$

where Φ is called generating functional. A drawback is that the choice of G in $\Phi[\mathscr{G}]$ it is known to over-screen the Coulomb interaction. The use of the unperturbed Green's function, G_0, under-screens the Coulomb interaction, and is also non-conserving. For investigation of spectral properties a possible loss of charge in the local DMFT cycle is often not noticeable and $\Phi[\mathscr{G}_0]$ sometimes shows better agreement with experimental spectra. When more intricate quantities than the spectral properties are investigated both versions have deficiencies. Our proposition is to use a partially renormalized Green's function as propagator, aiming to avoid both over and under screening. For the work performed in this thesis for example orbital moments are important, DFT often underestimates this, and with a good impurity solver the addition of on-site correlation effects can correct this [50]. Chadov et. al. proposes a scheme where both spectral properties and orbital moments come out well [51]. The scheme is based on the LDA+U approximation, with the additional SPT-FLEX diagrams (excluding the Hartree-Fock contribution) included afterwards. Different double counting (DC) is used for the LDA+U and SPT-FLEX parts of the calculation. The LDA+U is based on the full density matrix, and is hence conserving, whereas the SPT-FLEX version is based on the unperturbed local Green's function. Hence, the self-energy in this case is written as

$$\Sigma(i\omega_n) = \Sigma^{\text{HF}}[\widehat{\mathscr{G}}] - \Sigma^{\text{DC}^1} + \Sigma^{\text{SPT-FLEX}}[\widehat{\mathscr{G}}_0](i\omega_n) - \Sigma^{\text{HF}}[\widehat{\mathscr{G}}_0] - \Sigma^{\text{DC}^2}. \quad (3.30)$$

This scheme is not appealing to us mainly due to the introduction of additional free parameters in the two DC terms used and the inconsistency in the generating functionals . Instead we propose a new generating functional in $\Phi[\mathscr{G}^{\text{HF}}]$, where we define

$$\mathscr{G}^{\text{HF}} = [(i\omega_n + \mu) - \mathscr{H}_{0,\vec{R}} - \Delta(i\omega_n) - \Sigma^{\text{HF}}]^{-1}. \quad (3.31)$$

This approximation is also non-conserving, but the Hartree-Fock term is often dominant in the perturbation expression, hence this should be closer to a conserving approximation. We also eliminated the (possible) use of different double counting terms for the two self energies. The self-energy is calculated through

$$\Sigma(i\omega_n) = \Sigma[\hat{\mathscr{G}}^{\mathrm{HF}}](i\omega_n) - \Sigma^{\mathrm{DC}} \tag{3.32}$$

The resulting spin and orbital moment agrees just as well with experiments, for details see Paper I.
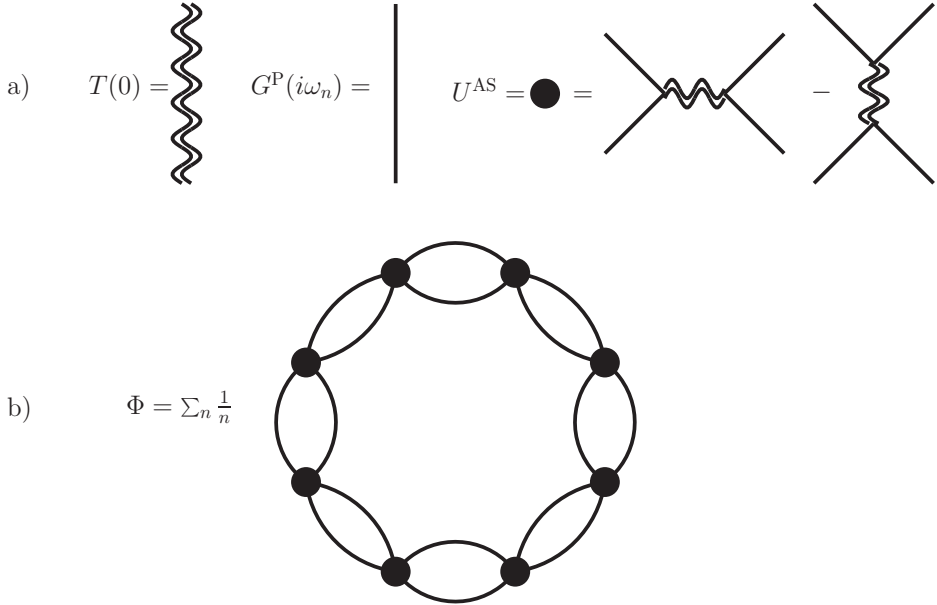
Figure 3.1: Schematic view of the diagrams involved in creating the generating functional for the SPT-FLEX impurity solver. a) displays the legend for the respective symbols, where P for the propagator $G^{\mathrm{P}}(i\omega_n)$ can be either (HF), (0) or full. The direction of the propagators depends on whether the particle-particle (PP) or particle-hole channels are considered. U^{AS} denotes the anti-symmetric vertex substituting the unscreened U when constructing the self-energy.

3.3.3   Solvers with approximate hybridization

Solvers approximating the hybridization function can be divided into two subclasses, both starting from an exact solution of the correlated orbitals for an atom, i.e. without hybridization, this is known as the Hubbard I approximation (HIA), it gives an accurate spectra in the limit of strong correlation and weak hybridization, $U/W >> 1$ [52]. Since the Hubbard 1 approximation works in

the atomic limit the only parts of the LDA+U Hamiltonian retained are the

$$\mathscr{H}_{\text{HIA}} = \mathscr{H}_{0,\vec{R}} + \frac{1}{2} \sum_{\vec{R},\xi_1,\xi_2,\xi_3,\xi_4 \in L_U} U_{\xi_1\xi_2\xi_3\xi_4} c^{\dagger}_{\vec{R},\xi_1} c^{\dagger}_{\vec{R},\xi_2} c_{\vec{R},\xi_3} c_{\vec{R},\xi_4} \qquad (3.33)$$

where $\mathscr{H}_{0,\vec{R}}$ is the LDA Hamiltonian projected on to the local basis set. The complete many-body basis for this Hamiltonian is small enough to set up and diagonalize directly. In terms of the AIM this equals ignoring the last two terms in Eq. 3.24. The so called Non-Crossing (NCA), One-Crossing (OCA), Two-Crossing (TCA) approximations etc. work with a perturbation expansion of the exact local solution in the hybridization function. They work well for strong to moderate correlation, $U/W > 1$, but are not able to describe the metal insulator transition correctly [53]. One can also include *auxiliary* orbitals, representing the hybridization with the bath in terms of extra orbitals in the atomic problem, this method goes under the name *Exact Diagonalization* (ED). This method is in principle exact (i.e. able to treat any range of U/W), as the number of auxiliary orbitals increase more of the hybridization is accounted for. However, the Hilbert space soon grows to prohibitive size, and in practice works for strong to moderate correlation, $U/W > 1$. Recently Hafermann *et. al.* presented a merger between the ED approach and perturbation theory that captures also the metal insulator transition and Kondo phenomena [54].

3.3.4 Double counting

A problem intrinsic to the LDA+DMFT procedure is that the Coulomb interaction is calculated twice for the correlated electrons, once in LDA, as they are part of the density on which the exchange correlation potential is calculated, and once when solving the impurity problem. Since the isolated exchange correlation contribution from the correlated electrons taken into account by LDA, and the LDA-like mean field part of the self-energy is not known, this cannot (as of now) be done exactly, several schemes have been suggested, but the range of applicability is still under dispute. When using schemes like GW+DMFT [55] this problem is completely circumvented. The main strategies how to estimate the double counted part of the interaction will be presented here. Due to the static nature of DFT, the double counting correction to the self-energy can be assumed to be frequency independent. The self-energy after correction reads

$$\Sigma_{\vec{R}}(i\omega_n) = \Sigma^{\text{AIM}}_{\vec{R}}(i\omega_n) - V^{\text{DC}}_{\vec{R}} \qquad (3.34)$$

where $\Sigma^{\text{AIM}}_{\vec{R}}(i\omega_n)$ is the result of the impurity solver and DC is the double counting of choice.

18

3.3.4.1 Around mean-field

The Around mean-field (AMF) double counting stems from Czyzyk and Sawatzky[56]. It is based on the assumption that LDA gives the correct total energy for a system without orbital polarization, and we can then subtract the static mean field contribution from the self-energy. This is reasonable for weakly correlated systems, but not exact as the orbital polarizations arising from LDA due to exchange interactions, spin-orbit coupling and crystal field splitting are neglected. The starting point is to redefine a density matrix without the charge $n = \text{Tr}(\rho)$ and magnetization $\vec{m} = \text{Tr}\vec{\sigma}\rho$ contributions

$$\tilde{\rho}_{\xi_1\xi_2} = \rho_{\xi_1\xi_2} - (\delta_{\xi_1\xi_2}n + \vec{\sigma}_{\xi_1\xi_2} \cdot \vec{m})/D \tag{3.35}$$

where D is the number of orbitals in the correlated subspace. This results in a correction to the self-energy

$$V_{\xi_1\xi_2}^{\text{AMF}} = \sum_{\xi_3\xi_4} (U_{\xi_2\xi_3\xi_1\xi_4} - U_{\xi_2\xi_3\xi_4\xi_1})\tilde{\rho}_{\xi_3\xi_4}. \tag{3.36}$$

3.3.4.2 Fully localized limit

The Fully localized limit (FLL) double counting assumes that the correlated orbitals are uniformly occupied in the LDA solution, and that the Coulomb interaction in the local orbitals can be represented by a constant times the total occupation of the correlated orbitals. This assumption holds when we assume integer occupation, i.e. in the insulating state. The potential is defined by

$$V_{\xi_1\xi_2}^{\text{FLL}} = V_{\xi_1\xi_2} - \left(\frac{U(2n-1)}{2} - \frac{J(n-1)}{2}\right)\delta_{\xi_1\xi_2} + \frac{J\vec{m} \cdot \vec{\sigma}_{\xi_1\xi_2}}{2} \tag{3.37}$$

where U and J in this notation is the spherically averaged Coulomb repulsion and intra-atomic exchange interaction.

3.3.4.3 Interpolation scheme

Even though most calculations use either one of these limits, the real system lies somewhere in between. This led Pethukov *et. al.* to develop an interpolationg scheme (INT) between these two limits [57]. AMF always gives a negative contribution to the energy, whereas FLL always gives a positive contribution. DFT is regarded to have a good total energy, but incorrect potential. This argument let us define an interpolation parameter α, determined in a self-consistent way minimizing the energy contribution from the double counting correction

$$\alpha = \frac{D\text{Tr}\tilde{\rho}^2}{Dn - n^2 - m^2}. \tag{3.38}$$

This method eliminates the choice of double counting for systems where the choice is not obvious, it also captures important magnetic features of Pu

monopnictides where AMF leads to a collapse of the magnetic moment for PuP, whereas FLL is unable to reproduce the non-magnetic solution for PuS. Only the INT DC reproduces the correct ground state for both compounds for a reasonable value of $U \sim 4\text{eV}$.

3.3.4.4 Static part of Σ

This double counting correction assumes that LDA describes the orbital average of the static part of the self-energy well for the separate spin-channels, i.e.

$$V^{\Sigma_0}_{\xi_1\xi_2\in s} = \frac{\delta_{\xi_1\xi_2}}{2l+1} \sum_{\xi_3\in s} \Sigma_{\xi_3,\xi_3}(0), \tag{3.39}$$

where s represents a spin-channel. This has proven to be reliable for moderately correlated systems like transition metals [58, 59] and actinide compounds [44].

4. Implementational aspects

To solve coupled partial differentials of the kinds presented in the previous chapter there are several methods available. In *ab-initio* material science by far the most common is to expand the operators in a well defined basis. This allows for a reformulation of the differential equation problem to an eigenvalue problem, which is much easier from a computational perspective.

4.1 DFT Basis sets

In the case of DFT we write the expansion of the wave functions in the basis functions ψ_l as

$$|\Psi_i\rangle = \sum_l c_l |\psi_l\rangle \tag{4.1}$$

Inserting this into Eq. (3.5) we get:

$$\sum_l c_l H^{\text{eff}} |\psi_l\rangle - \varepsilon_i \sum_l c_l |\psi_l\rangle = 0 \tag{4.2}$$

Multiplying from the left with $\langle \psi_k |$ yields:

$$\sum_l c_l \langle \psi_k | H^{\text{eff}} |\psi_l\rangle - \varepsilon_i \sum_l c_l \langle \psi_k |\psi_l\rangle = 0. \tag{4.3}$$

Defining $H_{kl} = \langle \psi_k | H^{\text{eff}} |\psi_l\rangle$, being a matrix element of the Hamiltonian and $O_{kl} = \langle \psi_k |\psi_l\rangle$, the overlap integral we can define the secular equation

$$\sum_l c_l (H_{kl} - \varepsilon_i O_{kl}) = 0 \tag{4.4}$$

Now the Kohn-Sham equation Eq. (3.5) has been transformed from a differential equation to a system of linear algebraic equations. By solving the eigenvalue problem Eq. (4.4) one obtains the energies, the coefficients c_l and thereby the solution of the Kohn-Sham equation. Generally the solution is obtained in an iterative fashion according to the variational procedure by Rayleigh and Ritz. A number of bases exist for this expansion, we need a basis set able to describe the system accurately, preferably with as small number of basis functions as possible. Many basis sets use the muffin-tin geometry, which emphasizes on the spherical symmetry of the potential close to the
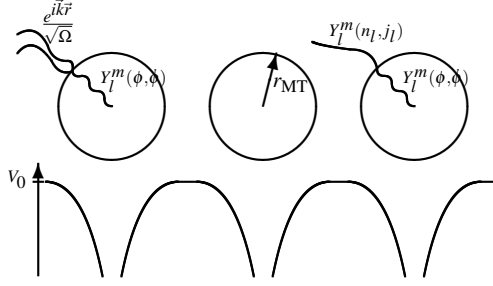
Figure 4.1: Schematic picture of the muffin-tins and the corresponding potential wells, V_0 denotes the muffin-tin zero and r_{MT} the muffin-tin radius. On the left hand side APW type basis functions are represented, on the right hand side LMTO type basis functions.

atoms in a crystal, and separates the problem into two domains. The external potential V_{ext} in Eq. (3.8) is represented in the unit cell by

$$V(\vec{r}) = \begin{cases} V_{\mathrm{MT}}(\vec{r}) & , |\vec{r}| < r_{\mathrm{MT}} \\ V_{\mathrm{I}}(\vec{r}) & , |\vec{r}| \geq r_{\mathrm{MT}}, \end{cases} \tag{4.5}$$

where MT represents muffin-tin region and I the interstitial region.

4.1.1 Linear muffin-tin orbitals

A brief introduction to the linear muffin-tin orbital (LMTO) [60] approach is given below, for an extensive review see the book by H.L. Skriver [61], for details about the particular implementation used, see J.M. Wills et. al. [62]. The method defines the basis functions as site centered, with a *head* inside the muffin tin, and a *tail* in the interstitial region. Moreover, a full-potential LMTO code must expand the cite centered basis functions around other sites, where the origin basis function is referred to as the *parent*. Formally the basis functions inside the MT sphere around some site τ are decomposed in terms of spherical harmonics times a radial function

$$\chi_{\tau,L}(\varepsilon,\vec{r}) = \mathscr{Y}_L(\widehat{\vec{r}})\phi_l(\varepsilon,r) \tag{4.6}$$

where τ refers to lattice cite, $L = (l,m_l)$, $\mathscr{Y}_L = i^l Y_{l,m}$, $\widehat{\vec{r}}$ is the angle and r is the length of $\vec{r}$, i.e. the distance to the center of site τ. The radial function $\phi_l(\varepsilon,r)$ is calculated as the solution to the radial Schrödinger equation,

$$\frac{\partial^2 (r\phi_l(\varepsilon,r))}{\partial r^2} = \left(\frac{l(l+1)}{r^2} + V_\tau(\vec{r}) - \varepsilon \right) r\phi_l(\varepsilon,r). \tag{4.7}$$

22

To remove the energy dependence the radial function is expanded around some linearization energy ε_ν to first order, defining

$$\phi_l(\varepsilon_\nu, r) \equiv \phi_l(\varepsilon_\nu, r)$$
$$\dot{\phi}_l(\varepsilon_\nu, r) \equiv \left. \frac{\partial \phi_l(\varepsilon, r)}{\partial \varepsilon} \right|_{\varepsilon = \varepsilon_\nu} \qquad (4.8)$$

$\phi_l(\varepsilon_\nu, r)$ and $\dot{\phi}_l(\varepsilon_\nu, r)$ are orthogonal to each other and the core states. The basis functions in the interstitial region is expanded in spherical harmonics times spherical waves with some wave number $\kappa_i^2 = V_I - \varepsilon_i$,

$$\chi_{I,L}(\varepsilon, \kappa, \vec{r}) = \mathscr{Y}_L(\widehat{\vec{r}}) y_l(\kappa, \vec{r}). \qquad (4.9)$$

The spherical waves are solutions to the Helmholtz equation,

$$\left(-\frac{d^2}{dr^2} + \frac{l(l+1)}{r^2} - \kappa^2 \right) r y_l(\kappa r) = 0, \qquad (4.10)$$

resulting in $y_l(\kappa r)$ being either of the two linearly independent solutions spherical Bessel ($j_l(\kappa r)$) or Neumann ($n_l(\kappa r)$) functions. If κ^2 is negative the solution is of the type Hankel function of the first kind. This results in the following basis functions

$$\chi_{\tau,L}(\varepsilon_\nu, \kappa, \mathbf{r}) = \mathscr{Y}_L(\hat{\mathbf{r}}) \begin{cases} \phi_l(\varepsilon_\nu, r) + \kappa \cot(\eta_l) J_l(\kappa r) & , r < r_{MT} \\ \kappa N_l(\kappa r) & , r \geq r_{MT} \end{cases} . \qquad (4.11)$$

As the basis functions are constrained to be continuous and differentiable in all space we introduce the phase shift η_l which fulfills

$$\cot(\eta_l(\varepsilon, \kappa)) = \frac{n_l(\kappa r)}{j_l(\kappa r)} \frac{D_l(\varepsilon) - \kappa D_{n_l}(\kappa)}{D_l(\varepsilon) - \kappa D_{j_l}(\kappa)} \qquad (4.12)$$

where $D_l(\varepsilon)$ are the logarithmic derivatives at the sphere boundary. J_L and N_L are *augmented* versions of the spherical Bessel and Neumann functions. J_L and N_L are required to be energy independent to first order around the linearization energy. This gives the spherical Bessel function the following shape:

$$J_l(\kappa r) = -\frac{\dot{\phi}(\varepsilon_\nu, r)}{\kappa \dot{\cot}(\eta_l(\varepsilon_\nu, \kappa))}, \qquad (4.13)$$

which is continuous and differentiable within the muffin-tin sphere and orthogonal to the core states. n_l is replaced by the augmented Neumann function N_l, using an expansion around the sites τ with $\vec{r}_\tau = \vec{r} - \vec{R}_{\tau'}$ they are defined as

$$N_L(\kappa, \vec{r}_\tau) = \begin{cases} 4\pi \sum_{L',L''} C_{LL'L''} J_{L'}(\kappa, (\vec{r}_{\tau'})) n_{L''}(\kappa, (\vec{r}_{\tau'})) & , |\vec{r}_{\tau'}| \leq r_{MT} \\ n_l(\kappa, \vec{r}_{\tau'}) & , |\vec{r}_{\tau'}| > r_{MT} \end{cases} \quad (4.14)$$

where $C_{LL'L''} = \int d\widehat{\vec{r}} Y_L(\widehat{\vec{r}}) Y_{L'}(\widehat{\vec{r}}) Y_{L''}(\widehat{\vec{r}})$ are Gaunt coefficients. It is common to use a basis with several κ for each l. Considering the disperse s- and p-valence bands it is common to use 3κ, (triple basis), while treating the narrower semi-core stats together with the d- and f-valence bands with 2κ, (double basis). Some implementations limits the the number of κ's to one (single basis), especially within the atomic sphere approximation only $\kappa = 0$ for all L's. The definition of the orbitals are covered by Eqs. (4.11) - (4.12), the Schrödinger equation is now solved according to Eq. (4.4). All LDA+DMFT calculations in this thesis are based on the FP-LMTO code RSPt [63].

4.1.2 Augmented plane-waves

The Augmented plane-wave (APW) [64, 65, 66] method uses the same geometry as the LMTO method, but the basis functions are defined as

$$\chi^{APW}_{\vec{k}+\vec{G}_m}(\vec{r}) = \begin{cases} \sum_L C_L(\vec{k}+\vec{G}_m) \psi_{\tau,L}(\varepsilon_v, \vec{r}) & , r < r_{MT} \\ e^{i(\vec{k}+\vec{G}_m)\vec{r})} & , r \geq r_{MT} \end{cases} \quad (4.15)$$

where $\psi_L(\varepsilon_v, \vec{r})$ are solutions to the radial Shrödinger equation just like in the LMTO case. The coefficients $C_L(\vec{k}+\vec{G}_m)$ are obtained by matching the value of the interstitial and the muffin-tin part of the wave-function. In contrast to the LMTO basis functions each APW has a discontinuous derivative at the sphere boundary, however the solution for the eigenstates minimizes the final discontinuity. The $\dot{\phi}(\varepsilon_v, r)$ is most conveniently included in the basis through local orbitals (lo). The main part of the calculations using the LDA+U method in this thesis are calculated with APW+lo as implemented in the Elk code [67].

4.2 Summary of Paper II: DMFT implementation

The accuracy of the DFT+DMFT scheme relies mainly on three quantities, the DFT basis, the quality of the impurity solver and the choice of correlated orbitals. The DFT basis and impurity solvers are already described in previous sections. Here we address the aspects of the implementation of the correlated orbitals, the mapping procedure and accuracy of Matsubara summations for temperature Greens functions. The general scheme is depicted in Fig. 4.2, where the quantities are denoted in operator form. The basis sets in which the operators are expanded will generally not be orthonormal, the following

relation for the operator and matrix form is used

$$
\begin{aligned}
\hat{A} &\to A \\
\hat{1} &\to O \\
\hat{A}\hat{B} &\to AO^{-1}B \\
\hat{A}^{-1} &\to OA^{-1}O
\end{aligned}
\tag{4.16}
$$

where O is the overlap matrix and $\hat{A}$, $\hat{B}$ are operators.
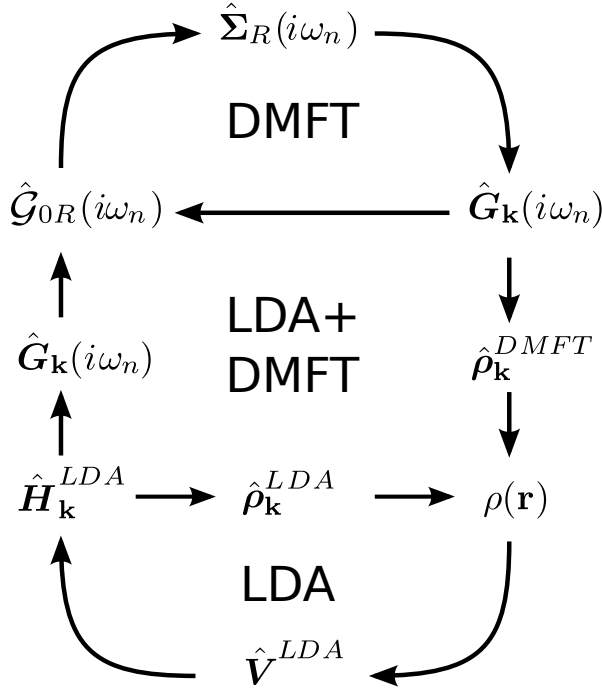
4.2.1 The mapping procedure

Local quantities, e.g. Hamiltonian, overlap is expanded in the basis functions $|\xi_i\rangle$ spanning the correlated subspace, the projectors are setup in two stages, first the projection coefficients between the LMTO basis χ_i and $|\xi_{\vec{R},L}\rangle$ are calculated. In the second step, if applicable, the local basis is rotated or reduced further to encompass e.g. crystal field or JJ orbitals according to

$$
\langle \xi_1 | \hat{T}^\dagger \hat{A} \hat{T} | \xi_2 \rangle = \sum_{\xi_3 \xi_4 \xi_5 \xi_6} T^*_{\xi_1} \mathscr{O}^{-1}_{\xi_3 \xi_4} A_{\xi_4 \xi_5} \mathscr{O}^{-1}_{\xi_5 \xi_6} T_{\xi_6 \xi_2}.
\tag{4.17}
$$

In the case that no extra transformation is made, T is simply the unit matrix and our transformation is defined by

$$A_{\xi_1\xi_2} = \langle\xi_1|\widehat{A}|\xi_2\rangle = \sum_{\vec{k},ij}\langle\xi_1|\chi_i^{\vec{k}}\rangle A_{i,j}^{\vec{k}}\langle\chi_j^{\vec{k}}|\xi_2\rangle = \sum_{\vec{k},ij} U_{i\xi_1}^{\vec{k},\vec{R}\dagger} A_{i,j}^{\vec{k}} U_{i\xi_2}^{\vec{k},\vec{R}}. \qquad (4.18)$$

The current implementation ha no restriction on the underlying lattice, e.g. a cluster of atoms represented in some of their cubic crystal field orbitals can be chosen.

4.2.2 Basis functions for the local problem

The choice of local orbitals is very intricate, it should, to as large extent as possible, be without spectral weight leakage, have pure angular character and be causal. The orbitals should also be reasonably localized if the mapping is to make sense. The spectral weight leakage can be quantified by looking at the overlap between the LMTO basis and the local basis,

$$\mathscr{O}_{\xi_1\xi_2} = \sum_{\vec{k},ij}\langle\xi_1|\chi_i\rangle (O_{\vec{k}}^{-1})_{ij}\langle\chi_j|\xi_2\rangle. \qquad (4.19)$$

which is ideally unity for a mapping, i.e. no spectral weight loss. The purity of the angular character is easily verified from the construction of the orbitals. Ref. [68] derives that the necessary and sufficient contition for causality is that the projectors are separable, i.e. $P^{\vec{k}}(ij,\vec{R},\xi_1\xi_2) = U_{i\xi_1}^{\vec{k},\vec{R}\dagger} U_{j\xi_2}^{\vec{k},\vec{R}}$, something that is true for the two types of basis functions for the local orbitals used in this implementation.

4.2.2.1 Orthogonalized LMTOs

The orthogonalized LMTO (ORT) basis is only possible to construct when a minimal basis (single κ) is used for the l-shell under consideration, in this case a simple Löwdin orthogonalization. The correlated orbitals are defined according to

$$\xi_i = \sum_{\vec{k},j} e^{i\vec{k}\vec{R}} \chi_{\vec{k},j} [\sqrt{O_{\vec{k}}^{-1}}]_{j,i} \qquad (4.20)$$

The basis is poorly localized, as the LMTOs extend into the interstitial and other spheres in a full potential LMTO code. Benefits are that there is no spectral weight leakage, as the overlap between the local orbitals and the DMFT is one by construction. This basis is poorly localized and the orbitals $|\vec{R},\xi\rangle$ do not have pure L character, however, there will be no leakage of spectral weight. This orbital construction is used by other LDA+DMFT implementation with charge self-consistency, e.g. Savrasov [69] or Pourovskii [70].

4.2.2.2 Muffin-tin heads

The second option is the Muffin-tin heads (MT) basis set, it is extremely localized with pure L character, and will be referred to the muffin-tin only (MT) orbitals, here we define the correlated orbitals as

$$\xi_{\vec{R},L}(\vec{r}) = \begin{cases} \mathscr{Y}_L(\widehat{\vec{r}})\phi_l(\varepsilon_{nu},r) & ,r < r_{MT} \\ 0 & ,r \geq r_{MT} \end{cases} . \tag{4.21}$$

this basis suffers from some spectral leakage, however, the mapping is usually $95\% - 100\%$ complete, i.e. the matrix

$$\mathscr{O} \sim \vec{1} \tag{4.22}$$

where I is the identity matrix[1]. We can also renormalize the basis set multiplying with $\mathscr{O}^{-1}$, or using just the diagonal components of $\mathscr{O}^{-1}$ resulting in something similar to the projector recommended in Ref. [68]. Renormalizing with the full matrix results in a small mixing of angular character, whereas renormalizing with the diagonal components results in pure angular character but polarization effects are diminished (i.e. occupations increase, but the off diagonal couplings are not increased). As the mapping is usually very close to complete for example spectral functions look the same regardless of renormalization. Magnetic moments and total occupations typically differs in the second or third significant digit.

4.2.3 Coulomb interaction in a spherical geometry

For a spherical geometry the Coulomb interaction can be rewritten into a convenient form, where

$$U_{\xi_1\xi_2\xi_3\xi_4} = \int d\vec{r}_1 d\vec{r}_2 \psi^*_{\vec{R},\xi_1}(\vec{x}_1)\psi^*_{\vec{R},\xi_2}(\vec{x}_2)g(\vec{r}_1 - \vec{r}_2)\psi_{\vec{R},\xi_3}(\vec{x}_1)\psi_{\vec{R},\xi_4}(\vec{x}_2) \tag{4.23}$$

is expanded in series of

$$g(\vec{r}_1 - \vec{r}_2) = \sum_{k=0}^{\infty} g_k(r_1,r_2)P_k(\cos(\theta_{12})). \tag{4.24}$$

where the radial part is integrated to

$$F^{(k)} = \int dr_1 dr_2 r_1^2 R_l^2(r_1)g_k(r_1,r_2)R_l^2(r_2)r_2^2 \tag{4.25}$$

---

[1]For the ORT basis set $\mathscr{O} \equiv I$ by definition

commonly referred to as Slater parameters [2]. Defining

$$c^k(m_1, m_2) = \left(\frac{4\pi}{2k+1}\right)^{1/2} \int d\Omega Y^*_{lm_1}(\Omega) Y_{k(m_1-m_2)}(\Omega) Y_{lm_2}(\Omega) \quad (4.26)$$

It is now straightforward to write U_{ijkl} as

$$U_{\xi_1\xi_2\xi_3\xi_4} = \delta_{s_1,s_3} \delta_{s_2,s_4} \delta_{m_1+m_2,m_3+m_4} \sum_{k=0}^{\infty} c^{(k)}(m_1,m_3) c^{(k)}(m_2,m_4) F^k \quad (4.27)$$

which with $q = m_1 - m_2$ can be written as

$$c^k(m_1, m_2) = (-1)^{m_1}(2l+1) \begin{pmatrix} l & k & l \\ 0 & 0 & 0 \end{pmatrix} \begin{pmatrix} l & k & l \\ -m_1 & q & m_2 \end{pmatrix} \quad (4.28)$$

resulting in

$$U_{\xi_1\xi_2\xi_3\xi_4} = \delta_{s_1,s_3} \delta_{s_2,s_4} \sum_{kq} (-)^{m_1+m_2+q} (2l+1)^2 \quad (4.29)$$

$$\times \begin{pmatrix} l & k & l \\ 0 & 0 & 0 \end{pmatrix}^2 \begin{pmatrix} l & k & l \\ -m_1 & -q & m_3 \end{pmatrix} F^{(k)} \begin{pmatrix} l & k & l \\ -m_2 & q & m_4 \end{pmatrix}.$$

From this form deduce that $F^0 = U$ represents the spherical part of the Coulomb interaction, The commonly used J is a linear combination of F^2, F^4 and F^6, for d-electrons the ratios are almost constant independent of material, whereas for f-electrons they are in general not. This results in a number of parameters, that are in principle possible to determine form experiment, but in practice this can be difficult due to lack of experimental data or the quality of the data. A way of reducing the number of free parameter is to use the Yukawa potential, $g = \frac{e^{-\lambda(\vec{r}-\vec{r}')}}{\vec{r}-\vec{r}'}$, here only the screening parameter λ is adjusted. Another benefit is that the ratio of the Slater parameters are calculated contrary to the common approach of choosing them separately, this method is explained extensively in paper IV. A more appropriate way to reduce the free parameters are to calculate the effective screening using the Random Phase Approximation (RPA) as suggested by Solovyev[50]. This implementation is presently lacking, but a comparison of the screening ratios of F^2, F^4 and F^6 to the ones calculated from the Yukawa potential would carry a great value. Note that in approaches like GW+DMFT this problem does not occur, as the screened Coulomb interaction is calculated within GW (often using RPA), also the issue of double counting is circumvented.

---

[2]The phase of the spherical harmonics is treated according to Condon and Shortley[71]

4.2.4 Integration of Matsubara Green's functions

The density matrix $\widehat{\rho}_{\vec{k}}^{DMFT}$ can be obtained from the Green's function as an infinite sum over all the Matsubara frequencies [72]

$$\widehat{\rho}_{\vec{k}} = \lim_{\eta \to 0^+} \lim_{N \to \infty} T \sum_{n=0}^{N} \left[\widehat{G}_{\vec{k}}(i\omega_n) e^{i\omega_n \eta} + \widehat{G}_{\vec{k}}^{\dagger}(i\omega_n) e^{-i\omega_n \eta} \right]. \tag{4.30}$$

The order of the limits can not be interchanged as the partial sums are only point wise convergent and not uniformly convergent with respect to η. To circumvent this problem the Green's function is decomposed into an analytical and a numerical part. To construct the analytical model Green's function a model self-energy $\Sigma_R^{an}(i\omega_n)$ is considered

$$\Sigma_R^{an}(i\omega_n) \equiv \widehat{\Sigma}_R(\infty) + \frac{V}{i\omega_n - \varepsilon}, \tag{4.31}$$

a reasonable function considering the analytic properties are the same as that of the Green's function. Now the partition of the Green's function can be defined as

$$\widehat{G}_{\vec{k}}^{an}(i\omega_n) = \left[i\omega_n \widehat{1} + \mu \widehat{1} - \widehat{H}_{\vec{k}}^{\mathrm{LDA}} - \sum_R \widehat{\Sigma}_R^{an}(i\omega_n) \right]^{-1} \tag{4.32}$$

$$\widehat{G}_{\vec{k}}^{num}(i\omega_n) = \widehat{G}_{\vec{k}}(i\omega_n) - \widehat{G}_{\vec{k}}^{an}(i\omega_n), \tag{4.33}$$

the density matrix can be split into two parts as $\widehat{\rho}_{\vec{k}} = \widehat{\rho}_{\vec{k}}^{an} + \widehat{\rho}_{\vec{k}}^{num}$, where

$$\widehat{\rho}_{\vec{k}}^{an} = \lim_{\eta \to 0^+} \lim_{N \to \infty} T \sum_{n=0}^{N} \left[\widehat{G}_{\vec{k}}^{an}(i\omega_n) e^{i\omega_n \eta} + \widehat{G}_{\vec{k}}^{an\dagger}(i\omega_n) e^{-i\omega_n \eta} \right] \tag{4.34}$$

$$\widehat{\rho}_{\vec{k}}^{num} = \lim_{\eta \to 0^+} \lim_{N \to \infty} T \sum_{n=0}^{N} \left[\widehat{G}_{\vec{k}}^{num}(i\omega_n) e^{i\omega_n \eta} + \widehat{G}_{\vec{k}}^{num\dagger}(i\omega_n) e^{-i\omega_n \eta} \right] \tag{4.35}$$

The analytical part $\widehat{\rho}_{\vec{k}}^{an}$ has a simple form but contains the logarithmic divergence of $\widehat{\rho}_{\vec{k}}$, while $\widehat{\rho}_{\vec{k}}^{num}$ converges uniformly [73]. The uniform convergence allows the order of the limits in Eq. (4.35) to be interchanged. With a minimal loss of accuracy the resulting sum can be truncated at some large cut-off Matsubara frequency $N_{\max}$, giving

$$\widehat{\rho}_{\vec{k}}^{num} \approx \sum_{n=0}^{N_{\max}} \left[\widehat{G}_{\vec{k}}^{num}(i\omega_n) + \widehat{G}_{\vec{k}}^{num\dagger}(i\omega_n) \right]. \tag{4.36}$$

The analytical part of the density matrix can still not be summed explicitly. By diagonalizing $\mu \widehat{1} - \widehat{H}_{\vec{k}}^{\mathrm{LDA}} - \sum_R \widehat{\Sigma}_R(i\omega_n)$ for a few n around $N_{\max}$, using the

model for the self-energy, the analytic Green's function is created by

$$G^{an}_{\vec{k},\chi_1,\chi_2}(i\omega_n) = \sum_m \frac{\langle \vec{k},\chi_1 | X^m_{\vec{k}} \rangle \langle X^m_{\vec{k}} | \vec{k},\chi_2 \rangle}{i\omega_n - \varepsilon^m_{1,\vec{k}} - \frac{V^m}{i\omega_n - \varepsilon^m_{2,\vec{k}}}} \tag{4.37}$$

where $\varepsilon_{1,m}$ and $|X^m_{\vec{k}}\rangle$ is eigenvalue and eigenvector m to $\widehat{H}^{\mathrm{LDA}}_{\vec{k}} - \sum_R \widehat{\Sigma}_R(\infty)$ and V^m and ε_2 is fitted to the decaying self-energy. Since $\widehat{\Sigma}_R(\infty)$ is hermitian the slow decaying tails are cancelled out by taking

$$\widehat{\Sigma}_R(\infty) \approx \widehat{\Sigma}^H_R(i\omega_{N_{\max}}) \equiv \frac{\widehat{\Sigma}_R(i\omega_{N_{\max}}) + \widehat{\Sigma}^\dagger_R(i\omega_{N_{\max}})}{2}. \tag{4.38}$$

The current implementation goes one step further and extrapolates $\widehat{\Sigma}^H_R(i\omega_n)$ to infinity from a least squares fit of a few data points around $N_{\max}$. Since $\widehat{\Sigma}^H_R(i\omega_n)$ is hermitian it can be expanded in orders of ω_n^{-2}, so the first order fit has an error proportional to $\omega_{N_{\max}}^{-4}$. Now the two residues for each eigen function can be summed, the approximation is that the eigen representation does not change for high energies.

Expectation values of statical quantities can be evaluated directly from the density matrix, e.g. spin moment $\langle \widehat{s_z} \rangle = \mathrm{Tr}(\widehat{s_z}\widehat{\rho})$ or single particle energy $\langle \widehat{H}_{\mathrm{LDA}} \rangle = \mathrm{Tr}(\widehat{H}_0\widehat{\rho})$.

The total energy is derived by equation of motion of the Greens function and the definition of the Hamiltoninan in eq. 3.21

$$\langle \frac{\partial}{\partial \tau} \widehat{G}(\tau) \rangle = \langle \widehat{H}_{\mathrm{LDA}} \rangle + 2\langle \widehat{H}_U \rangle \tag{4.39}$$

where τ is the imaginary time. Fourier transforming the left hand side using the definition of the Greens function we obtain

$$\mathrm{Tr}[\omega \widehat{G}(\omega)] = \mathrm{Tr}[\widehat{\Sigma}(\omega)\widehat{G}(\omega)] + \mathrm{Tr}[\widehat{H}_{\mathrm{LDA}}\widehat{G}(\omega)]. \tag{4.40}$$

Where the frequency independence of $\widehat{H}_{\mathrm{LDA}}$ allows the single particle energies to be evaluated by

$$Tr[\widehat{H}_{\mathrm{LDA}}\widehat{\rho}] \tag{4.41}$$

and the many-body correction, the *Galitskii-Migdal* energy [74, 72]

$$E_{\mathrm{GM}} = \mathrm{Tr}[\widehat{\Sigma}(\omega)\widehat{G}(\omega)] \tag{4.42}$$

is evaluated using the same procedure as the density matrix.

4.3 Integration methods

With the reciprocal space representation of the wave function according to Eq. 2.11 the expectation value of an operator $\widehat{X}$ is calculated by integrating the matrix elements over the Brillouin zone. Defining

$$X_i(\vec{k}) = \langle \psi_i(\vec{k})|\widehat{X}|\psi_i(\vec{k})\rangle \tag{4.43}$$

the expectation value is

$$\langle \widehat{X}\rangle = \sum_i \frac{1}{\Omega_{BZ}} \int_{BZ} X_i(\vec{k})\Theta(\varepsilon_i - \mu)d\vec{k}, \tag{4.44}$$

where i is the band index, Ω_{BZ} is the volume of the Brillouin zone, $X_i(\vec{k})$ is the function to be integrated and $\Theta(\varepsilon_i - \mu)$ is a step function. Since a discrete mesh of k-points samples the (continuos) reciprocal space convergence needs to be tested thoroughly. There are different schemes for integration with rather different convergence behavior, the intuitive way (for 0K temperature) would be to use a step function

$$\langle \widehat{X}\rangle = \sum_i \frac{1}{\Omega_{BZ}} \sum_{\vec{k}} w_{\vec{k}} X_i(\vec{k})\Theta(\varepsilon_i - \mu)d\vec{k}, \tag{4.45}$$

where $w_{\vec{k}}$ is the symmetry reduced weight of the k-point. This leads to very slow convergence as the occupancy jumps from 0 to 1 at the Fermi level. To circumvent this one frequently uses either smearing quadratures (Methfessel-Paxton, Fermi smearing etc.) or interpolation schemes (tetrahedron method, cubic interpolation etc.).

4.3.1 Smearing quadratures

In this approach the step functions is replaced with a smooth function $f(\sigma, \varepsilon_i - \mu)$. The integral now takes the shape of

$$\langle \widehat{X}\rangle = \sum_i \frac{1}{\Omega_{BZ}} \sum_{\vec{k}} w_{\vec{k}} X_i(\vec{k}) f(\sigma, \varepsilon_i - \mu)d\vec{k}. \tag{4.46}$$

One popular choice is so-called temperature smearing, defining $x = \frac{\varepsilon - \mu}{\sigma}$ the definition of $f(x)$ simply takes the form of the Fermi-Dirac distribution[75]

$$f(x) = \frac{1}{e^x + 1} \tag{4.47}$$

where $\sigma = \beta^{-1} = k_b T$. Using smearing quadrature yields exactly the same result as using temperature Greens-functions, and can hence be used as a test of the implementation.

Another popular choice proposed by Methfessel and Paxton is to use Hermite's functions [76], the resulting $f(x)$ is defined through the recursive formula

$$f_0(x) = \frac{1}{2}\text{erfc}(x) \tag{4.48}$$

$$f_N(x) = f_0(x) + \sum_{n=1}^{N} A_n H_{2n-1}(x) e^{-x^2} \tag{4.49}$$

where $\text{erfc}(x) = \int_{-\infty}^{x} e^{-t^2} dt$ is the complementary error function, $H_{2n-1}(x)$ is an Hermite function and A_n are expansion coefficients arising from expanding the delta function in in therms if Hermite functions. This scheme show good convergence properties for metals, but suffers from unphysical effects of negative occupation for higher orders. A correction to this is proposed by Marzari and Vanderbilt, approximating the delta function by a Gaussian times a polynomial [77].

All smearing methods introduce another caveat; they are not variational with respect to the total energy E. This means that the ground state energy does not minimize E, but instead a generalized free energy $F = E - TS = E - \sum_i \sigma S(f(x_i))$. For Fermi smearing this translates to

$$S(f) = -(f\ln(f) + (1-f)\ln(1-f)) \tag{4.50}$$

In the case of DMFT the entropy contribution is more difficult to calculate, Kotliar *et al* proposes a numerical temperature integration scheme which requires well converged total energies for a number of temperatures. However, for sufficiently high temperature we can use the von Neumann entropy

$$S = -k_B \text{Tr}(\rho \ln \rho), \tag{4.51}$$

where ρ is the density matrix in the LDA basis, for a mean field estimate. For solvers where the full Hilbert space is represented (e.g. Hubard 1) the von Neuman entropy is accurate in the many particle basis.

4.3.2 The tetrahedron method

One of the most used integration schemes for metals is the linear tetrahedron method [78](with Blöchl corrections [79]). This is due to superior convergence properties compared to smearing based quadratures (e.g. Gaussian and Fermi quadratures). The tetrahedron method divides the reciprocal space into tetrahedrons, most often following Fig. 4.2 or similar schemes with equal volume for all tetrahedrons. For all corners of a tetrahedron the function value is known, hence we can construct an interpolation scheme within the tetrahe-

dron. The results in an integral on the form

$$\langle \widehat{X} \rangle = \sum_i \frac{1}{\Omega_{\text{BZ}}} \sum_{\vec{k}} w_{i,\vec{k}} X_i(\vec{k}) d\vec{k}, \tag{4.52}$$

where the weights $w_{i,\vec{k}}$ are calculated by interpolating the band i within all tetrahedrons where k is a corner. In general the tetrahedrons are setup using a scheme which makes the integration anisotropic, e.g. when calculating the number of particles for a magnetic system including spin-orbit coupling two supposedly equivalent directions will give different results, as charge must be conserved to avoid issues with the Madelung energy this will manifest itself in different Fermi levels, see Fig. 4.3 for an example. The current
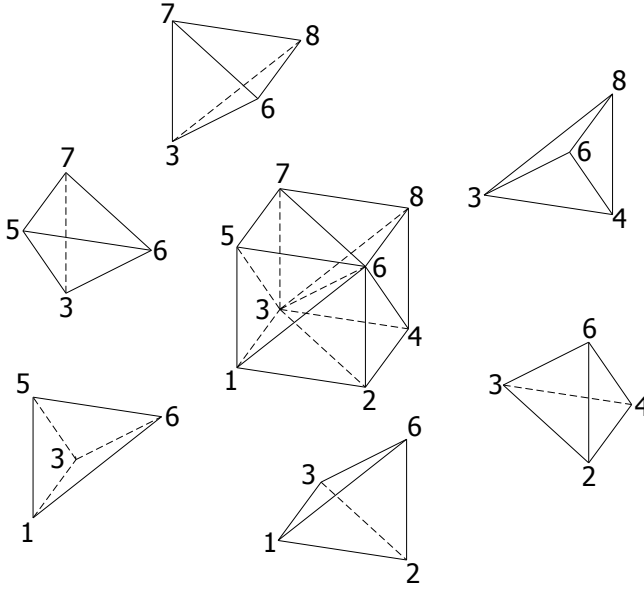
Figure 4.2: Schematic picture of a cube divided in tetrahedrons, following the work of P Blöchl[78]. The division procedure can be assigned an orientation through the body diagonal. As the tetrahedrons are anisotropic also the result of the integration will have minor anisotropies.

implementation is able to handle any k-mesh but the standard generator is based on the k-point sampling scheme proposed by S. Froyen [80], where the k-points are distributed on a cubic mesh, and mapped onto the reciprocal space of the crystal.
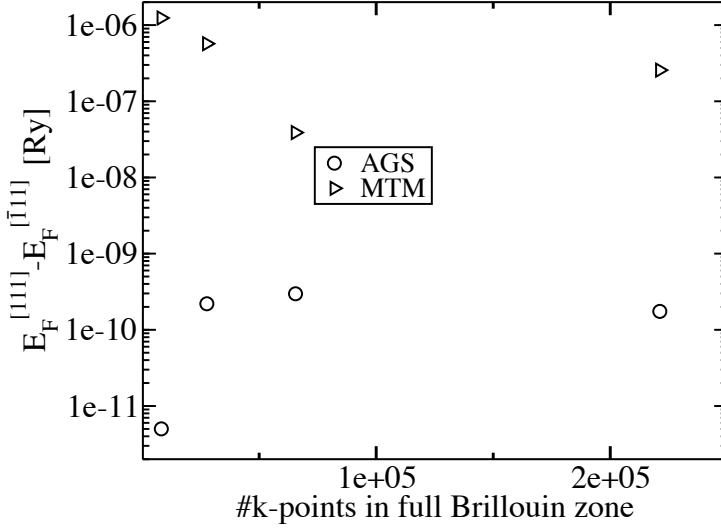
Figure 4.3: The figure shows the difference in the Fermi level between crystallographically equivalent directions, the [111] direction is the body diagonal used as origin for dividing the cube into tetrahedrons. The results are computed from the same potential and linearization energies (converged without spin-orbit coupling), subsequently spin-orbit interaction is turned on and one iteration is done for each crystallographic direction. The difference due to the anisotropic tetrahedrons are 2-3 orders of magnitude larger than the differences are when using the adaptive gaussian smearing scheme, and is hence the dominant numerical noise in the calculation. The trial system is bcc Fe.

4.3.3 Summary of Paper III: The Adaptive Gaussian Smearing method for integration

As presented in the sections on the tetrahedron method and the smearing methods it is hard to get reliable numbers on small quantities which are sensitive to the position of the fermi-level. For instance magneto crystalline anisotropy energies (MAEs) for cubic $3d$ transition metals needs convergence in the order of 1e-7 eV, which is smaller then the error introduced by the asymmetries in the tetrahedron method, and generally requires a very tedious convergence test of both k-point mesh and smearing width for the smearing methods (however, for Fermi smearing one can argue that the fermi level obtained is for a certain temperature). For these reasons we developed the Adaptive Gaussian Smearing (AGS) scheme, which, despite the name, works for any of the smearing methods described in the previous section. It is derived from the argument that

the smearing should decrease as the k-mesh increases. The energy resolution for a given band is determined by the density of k-points though

$$\Delta E = \frac{dE}{dk}\Delta k. \tag{4.53}$$

The energy resolution should be such that there is a smooth connection between each k-point while retaining resolution of individual eigenvalues. For Gaussian smearing a reasonable value is $\Delta E = 2\sigma$, where σ is the standard deviation. The k-point resolution is calculated as the radius of a sphere whose volume is the average volume per k-point

$$\Delta K = \left(\frac{3}{4\pi} \frac{V_{\text{BZ}}}{n_k} \right)^{1/3}. \tag{4.54}$$

We still have to evaluate $\frac{dE}{dk}$, this is done by assuming a free-electron dispersion of the bands, $E(k) = \frac{k^2}{2m^*}$. Using the electron rest-mass is in most cases a pessimistic guess, as most metals are not free electron like. This is evaluated at the Fermi k-vector $k_{\text{F}} = \sqrt{2E_{\text{F}}} = \sqrt{2W}$, where W is the width of the occupied band. Now we have an expression for the smearing that depends on the number of k-points used in the sampling,

$$2\sigma = \frac{\sqrt{2W}}{m^*} \left(\frac{3}{4\pi} \frac{V_{\text{BZ}}}{n_k} \right)^{1/3}. \tag{4.55}$$

The effective mass parameter m^* can be used as a tuning parameter to speed up convergence, but regardless of choice the same result will be achieved. The same is true for the choice of $\Delta E = 2\sigma$, here the factor 2 can be included in m^*, as we will have convergence to the same result. In the limit of a dense mesh (infinite number of k-points) the step-function is be retained as $\sigma \to 0$, but convergence issues does not arise here as the weight of each k-point is approaching zero.

5. Multipolar analysis

The electronic occupations can polarize either in spin space, resulting in a spin-moment, or in orbital space, resulting in some orbital ordering effect. If spin and orbital degrees of freedom are coupled we can also have combinations of these, resulting in four possibilities, charge density multipoles, spin density multipoles, charge currents and spin currents. The most common polarizations to consider are the spin and orbital moments, however, these are a few of the lowest order of polarizations possible for each l-shell. In fact, the local density matrix has $(2(2l+1))^2$ independent elements, of which we usually consider only 7, occupancy n, spin moment $\vec{s}$ and orbital moment $\vec{l}$. For many properties of weakly correlated metals the LDA determines these quantities reasonably well, however higher order polarizations are largely underestimated, and if we consider strongly correlated materials we have to include an orbital dependence in the exchange correlation, e.g. through LDA+U or LDA+DMFT. Analysis of higher order ordering effects are not straightforward, the common route is to project on a basis with some clear physical meaning, for example projecting to the $l, m_{\vec{s}}$ will show the l resolved exchange splitting, the J, m_J basis shows if you have a strong coupling between spin and orbital space[1] and projection onto the crystal harmonics indicates the splitting caused by the crystal electric field. The basis where the off-diagonal elements of the density matrix is minimal indicates what physical phenomena that dominates the system, however, not in detail. Generally the eigenvectors of the the density matrix shows no clear preference for either phenomena, and are difficult to analyze. A reliable analysis should include not only occupational polarization, but also the contribution to the energy, preferably both static and dynamic effects should be taken into account. From experimental perspective multipolar ordering is difficult to probe directly, as a detailed picture of the local electronic structure is needed. Experimental techniques used to detect multipolar ordering include resonant x-ray scattering (RXS), non-resonant x-ray diffraction (XRD) and neutron diffraction, for a review consider Santini et. al. [81] and references therein.

---

[1]The spin-orbit coupling $\xi \sum_i \vec{l}_i \cdot \vec{s}_i$ is diagonal in the J, m_J basis.

5.1 Multipole tensor formalism

In relation with spectroscopy it is common to describe polarizations of the charge- and spin-densities in terms of multipoles derived from $\vec{l}$ and $\vec{s}$ operators. Following G. van der Laan the lowest order tensors, together with their physical interpretation, are shown in tab. 5.1 [82]. It is now clear that it

Table 5.1: *Relation between spherical tensors and standard ground state operators.* $S_z = \sum_i s_{z,i}$, $L_z = \sum_i l_{z,i}$, $T_z = \frac{1}{4}\sum_i(3[l_z(\vec{l}\cdot\vec{s})] - 2l^2 s_z)_i$, $Q_{zz} = \sum_i(l_z^2 - \frac{1}{3}l^2)_i$, $P_{zz} = \sum_i(l_z s_z - \frac{1}{3}\vec{l}\cdot\vec{s})_i$ *and* $R_{zz} = \frac{1}{3}\sum_i[5l_z(\vec{l}\cdot\vec{s})l_z - (l^2-2)\vec{l}\cdot\vec{s} - (2l^2+1)l_z s_z]_i$

	w^{kpr}
Number operator	$w^{000} = n$
Isotropic spin-orbit coupling	$w^{110} = (ls)^{-1}\sum_i \vec{l}_i\cdot\vec{s}_i$
Spin moment	$w_0^{011} = -s^{-1}S_z$
Orbital moment	$w_0^{101} = -l^{-1}L_z$
Magnetic dipole	$w_0^{211} = -(2l+3)l^{-1}T_z$
Quadropole moments	$w_0^{202} = 3[l(2l-1)]^{-1}Q_{zz}$
	$w_0^{112} = 3l^{-1}P_{zz}$
	$w_0^{312} = 3[(l-1)(2l-1)]^{-1}R_{zz}$

becomes quite cumbersome to derive the expression for the higher order multipoles, hence a general method will simplify implementation a great deal. We will denote trace over m_l, m_s as Tr_L, and trace over Matsubara frequencies as $\mathrm{Tr}_{i\omega_n}$. Making our way towards expressing the local density matrix in terms of multipoles we start by introducing the multipolar charge distribution

$$w_x^k = \mathrm{Tr}_L \Gamma_x^k \rho \tag{5.1}$$

where

$$\Gamma_x^k \equiv \langle m_b | \widehat{\Gamma}_x^k | m_a \rangle = (-1)^{l-m_b} n_{lk}^{-1} \begin{pmatrix} l & k & l \\ -m_b & x & m_a \end{pmatrix}. \tag{5.2}$$

The constant n_{lk} is chosen according to the preferred normalization, we follow the notation of G. van der Laan [82], that is

$$n_{lk} = \frac{(2l)!}{\sqrt{(2l-1)!(2l+k+1)!}} \tag{5.3}$$

The spin dependence is introduced though

$$w_{xy}^{kp} = \mathrm{Tr}_L \Gamma_{xy}^{kp} \rho = \mathrm{Tr}_L \Gamma_x^k \Gamma_y^p \rho \tag{5.4}$$

with

$$\Gamma_y^p \equiv \langle s_b | \widehat{\Gamma}_y^p | s_a \rangle = (-1)^{s-s_b} n_{sp}^{-1} \begin{pmatrix} s & p & s \\ -s_b & y & s_a \end{pmatrix}. \tag{5.5}$$

Using the orthogonality properties of the 3j-symbols

$$\sum_{lm} [l] \begin{pmatrix} l_1 & l & l_2 \\ m_a & m & m_b \end{pmatrix} \begin{pmatrix} l_1 & l & l_2 \\ m_c & m & m_d \end{pmatrix} = \delta(m_a, m_c) \delta(m_b, m_d) \tag{5.6}$$

where $[l] = (2l+1)$, invertability of the transform can be confirmed. Resulting in

$$\rho_{ab} = \sum_{kx} [k] n_{lk} (-1)^{m_b - l} \begin{pmatrix} l & k & l \\ -m_b & x & m_a \end{pmatrix} \sum_{py} [p] n_{sp} (-1)^{s_b - s} \begin{pmatrix} s & p & s \\ -s_b & y & s_a \end{pmatrix} w_{xy}^{kp} \tag{5.7}$$

We now have an expression for charge and spin multipoles in terms of expectation values of easily obtainable operators. Considering the expression for the Coulomb interaction in section 4.2.3 we derive an expression for the Hartree and Exchange energy contributions for each multipole tensor. Starting with the Hartree term

$$E_{\mathrm{H}} = \frac{1}{2} \sum_{abcd} \rho_{ab} U_{abcd} \rho_{cd} \tag{5.8}$$

and the expressions derived for density matrix and Coulomb interaction respectively the tensor moment resolved energy is

$$E_{\mathrm{H}} = \sum_{2k=0}^{4l} \frac{(2l+1)^2}{2} \sum_k n_{nl}^2 \begin{pmatrix} l & k & l \\ 0 & 0 & 0 \end{pmatrix}^2 F^{(k)} w^{k0} \cdot w^{k0}. \tag{5.9}$$

In a similar manner the exchange energy

$$E_{\mathrm{X}} = \frac{1}{2} \sum_{abcd} \rho_{ab} U_{abcd} \rho_{dc} \tag{5.10}$$

is expressed as

$$E_{\mathrm{X}} \quad = -\sum_{2k=0}^{4l} F^{(k)} \sum_{k_1=0}^{2l} \frac{(2l+1)^2(2k_1+1)}{4} (-1)^{k_1} n_{lk}^2 \begin{pmatrix} l & k & l \\ 0 & 0 & 0 \end{pmatrix} \tag{5.11}$$

$$\times \quad \begin{Bmatrix} l & l & k_1 \\ l & l & k \end{Bmatrix} w^{kp} \cdot w^{kp}. \tag{5.12}$$

We now have a complete analysis tool for the density matrix, including static energy contribution from LDA+U resolved in tensor moments. For systems with strong spin-orbit coupling we have coupling between the spin and orbital

degrees of freedom, this results in a coupling of the indices k and p and the irreducible tensors given in table 5.1

$$w_t^{kpr} = \underline{n}_{kpr}^{-1} \sum_{xy} (-1)^{k-x+p-y} \begin{pmatrix} k & r & p \\ -x & t & -y \end{pmatrix} \tag{5.13}$$

where

$$\underline{n}_{kpr} = i^g \left(\frac{(g-2k)!(g-2p)!(g-2r)!}{(g+1)!} \right)^{1/2} \frac{g!!}{(g-2k)!!(g-2p)!!(g-2r)!!}. \tag{5.14}$$

In turn the expectation value of the $k - p$-coupled operator

$$\Gamma_{t,ab}^{kpr} = \underline{n}_{kpr}^{-1} n_{lk}^{-1} n_{sp}^{-1} (-1)^{-m_a+l-s_a+s+k+p} \sum_{xy} (-1)^{-x-y} \tag{5.15}$$

$$\times \begin{pmatrix} l & k & l \\ -m_a & x & m_b \end{pmatrix} \begin{pmatrix} s & p & s \\ -s_a & y & s_b \end{pmatrix} \begin{pmatrix} k & r & p \\ -x & t & -y \end{pmatrix}$$

The transformation is complete, and the operator Λ_t^{kpr} is defined as the inverse transform matrix through

$$\Lambda_t^{kpr} = (-1)^{k+r+p} [kpr] \underline{n}_{kpr} n_{lk} n_{sp} \Gamma_t^{kpr} \tag{5.16}$$

$$\mathrm{Tr} \Gamma_t^{kpr} \Lambda_{-t'}^{k'p'r'} = (-1)^t \delta_{kk'} \delta_{pp'} \delta_{rr'} \delta_{tt'} \tag{5.17}$$

To include dynamic effects we resort to DMFT, where the local density matrix is substituted for the local Green's function. All operators are expressed as matrix representations in the $|l, m_l, m_s\rangle$ basis if nothing else is stated. The mapping of the Green's function to tensor moments is done in similar fashion as the density matrix, defining the Green's function expressed in the full irreducible tensor

$$\mathscr{W}_t^{kpr}(i\omega_n) = \mathrm{Tr}_L \Gamma_t^{kpr} G(i\omega_n) \tag{5.18}$$

where the Green's function is retained from the tensor representation throug

$$G_{ab}(i\omega_n) = \sum_{kpr} \vec{\Lambda}_{ab}^{kpr} \vec{\mathscr{W}}^{kpr}(i\omega_n) \tag{5.19}$$

The occupational spherical tensors in tab. 5.1 is recovered through the trace over Matsubara frequencies

$$w_t^{kpr} = \mathrm{Tr}_\omega \mathscr{W}_t^{kpr}(i\omega_n) \tag{5.20}$$

and the density matrix

$$\rho_{ab} = \mathrm{Tr}_\omega G_{ab}(i\omega_n) = \sum_{kpr} \vec{\Lambda}_{ab}^{kpr} \vec{w}^{kpr} \tag{5.21}$$

40

Considering the Dyson equation

$$\Sigma(i\omega_n) = G_0^{-1}(i\omega_n) - G^{-1}(i\omega_n), \tag{5.22}$$

we argue to use the same transformation for the self energy.

$$\mathcal{V}_t^{kpr}(i\omega_n) = \mathrm{Tr}_L \Gamma_t^{kpr} \Sigma(i\omega_n) \tag{5.23}$$

The energy contribution from the local problem is calculated following the Galitskii-Migdal expression

$$E_{\mathrm{GM}} = \frac{1}{2}\mathrm{Tr}_{L,\omega}\Sigma(i\omega_n)G(i\omega_n) \tag{5.24}$$

In practice this is evaluated using exactly the same routines as in the non-projected Galitskii-Migdal energy, the difference being that his is done kpr resolved, i.e.

$$E_{\mathrm{GM}}^{kpr} = Tr_{L,\omega} \sum_{t=-r}^{r} \left(\Lambda_t^{kpr} \mathcal{V}_t^{kpr}(i\omega_n) \Lambda_{-t}^{kpr} \mathcal{W}_{-t}^{kpr}(i\omega_n) \right) \tag{5.25}$$

5.2 Physical interpretation

As seen in tab. 5.1 there is an apparent physical meaning to the tensors, in general we have for even k that $\vec{w}^{k0}$ represents the k'th multipole of charge-, and $\vec{w}^{k1}$ represents the k's multipole of magnetization densities for a certain l-shell of a lattice site. Odd k breaks time reversal symmetry in charge-, and odd p breaks time reversal symmetry in spin-space, hence the tensors describe currents $p = 0$ and spin currents $p = 1$. In total the time reversal symmetry is broken if $k + p$ is odd, the coupled index r refers to the total rank of the multipole. Since a physical fermionic density matrix is hermitian, with eigenvalues $0 \leq e_v \leq 1$ it must obey

$$\mathrm{Tr}[\rho] \geq \mathrm{Tr}[\rho^2] \tag{5.26}$$

the polarization of the system is constrained according to [2]

$$\vec{w}^{000} \geq \sum_{kpr} \frac{[kr]}{2} |\underline{n}_{kpr}|^2 n_{lk}^2 \vec{w}^{kpr} \cdot \vec{w}^{kpr}. \tag{5.27}$$

---

[2]Here we use the fact that $\mathrm{Tr}\rho = \vec{w}^{000}$, the scalar product between tensor moments is defined as $\vec{w}^{kpr} \cdot \vec{w}^{kpr} \sum_{t=-r}^{r} w_t^{kpr} w_{-t}^{kpr}$.

Since $\vec{w}^{000} = \mathrm{Tr}\rho$ is the occupation of the system, we can write the equation as [3]

$$\vec{w}^{000} \geq \frac{1}{2[l]}\vec{w}^{000} \cdot \vec{w}^{000} + \sum_{kpr \neq 000} \frac{[kr]}{2}|\underline{n}_{kpr}|^2 n_{lk}^2 \vec{w}^{kpr} \cdot \vec{w}^{kpr}. \qquad (5.28)$$

Introducing n_e, n_h as the number of electrons and the number of holes respectively, some rearrangement leads to

$$n(2[l]-n) = n_e n_h \geq \sum_{kpr \neq 000} [lkr]|\underline{n}_{kpr}|^2 n_{lk}^2 \vec{w}^{kpr} \cdot \vec{w}^{kpr} = \sum_{kpr \neq 000} \pi^{kpr} \quad (5.29)$$

where π^{kpr} is defined as the polarization of the kpr channel. Occupation following Hunds rules results in a fully polarized system leading to idempotency and equality in the equation, for itinerant systems we have partial polarization, but using the analysis tool presented here it is clear what channel is preferred.

5.3 Summary of Papers IV-XIII

This section serves as a short summary of the papers on multipoles and general spin and orbital polarization.

5.3.1 IV, V: Development of the multipole formalism and applications to actinide compounds

Paper IV focuses on the reduction of "free" parameters in LDA+U calculation, and assesses the calculation in terms of multipolar ordering. For the test cases PuS and PuP it is found that the interpolation double counting is crucial for describing the magnetism in a uniform manner. Using the AMF double counting the magnetic moment is quenched for both compounds for low values of U, whereas the FLL double counting is unable to reproduce the non magnetic ground state of PuP for any realistic value of U. Using INT double counting we obtain the experimental magnetic structure for a range of U 3.5eV. Systematic calculations are performed for a number of U, Np and Pu compounds with various degree of f-electron localization, we found that these materials are not so well understood through arguments based on Hund's rules, in fact the role of the spin-moment is marginalized due to polarization of higher order multipoles.

Since the formalism introduced in Paper IV only deals with static approximations, whereas dynamic effects are known to be important in many of the compounds we study, we extend the formalism in paper V to include dynamic effects through DMFT. Resorting to many body methods have the potential

---

[3]The constants $n_{l0}^2 = [l]^{-1}$ and $\underline{n}_{000}^2 = 1$.

gain of even less "free" parameters, as there are well developed methods for calculating the screened coulomb interaction from first principles (note that these are also possible to use with LDA+U, but then no local screening is provided by Hartree Fock). The double counting still remains an issue unless one takes one further step and cut the ties with DFT, using for example GW for the itinerant electrons. Another issue is that solvers using density-density approximation penalize many of the polarization channels in the sense that their energy contribution is simply zero. On the other hand, solvers describing the interaction with full U-matrix are in general not applicable for all ranges of U/W (SPT-FLEX, Hubbard I, ED), or they are exceedingly computationally demanding (full-U CT-QMC). The first case study is the δ-phase of Pu, where we know that the branching ratio of white light $4d \rightarrow 5f$ ($\vec{w}^{110} = \frac{2}{3}\langle \vec{l} \cdot \vec{s} \rangle$) transitions from the LDA ground state is only -2.4 [83] with a large spin moment, whereas the experimental number for δ-Pu is ∼-5.4 for an f^5 configuration with no magnetic moment [84] . Previous calculations of the δ phase shows similar numbers, but using the density-density CT-QMC solver, hence the solution is reached from a non-magnetic LDA ground state.[85]. Calculations using LDA+U indicates the magnetic moment vanishes due to the fact that the exchange energy goes into the $\vec{w}^{110}$ channel, but the resulting branching ratio is overestimated with about 20%. DMFT calculations attribute the vanishing moment to the Kondo effect, but the large spin-orbit current increase is also seen. No energy contributions are calculated, so the underlying reason is not clear. We establish that the energy contribution from polarizing $\vec{w}^{110}$ is about 0.4Ry, i.e. a much larger contribution than that of the proposed coherence scale attributed to the Kondo effect with $K_T \sim 800K$, i.e. about 5mRy [86]. We also conclude that there is a mass enhancement indicating both effects are present, moreover, the best suitable solver for this problem would be the full U CT-QMC, which unfortunately takes prohibitively long time to converge with the computational resources at hand.

5.3.2 VI: Polarization of an open shell in the presence of spin-orbit coupling

In paper VI we investigate spontaneous symmetry breaking in presence of strong spin-orbit coupling. The density matrix of a crystalline solid always shows some polarization due to directional bonds that typically give rise to higher order charge multipoles. This kind of polarization is by us referred to as induced, as it is an effect of the geometry of the problem. Spontaneous polarization includes time-reversal symmetry breaking, according to Hund's rules this occurs first and foremost in the $\vec{w}^{011}$ channel. However, strong spin-orbit coupling makes this unfavorable as the possibility of larger energy gains are possible by polarizing higher order multipoles. We performed large scale investigations of actinide compounds, from which we formulated the empiri-

cal *Katt's rules*, a set of rules complementary to Hund's, valid for the strong spin-orbit coupling regime, see Tab. 5.2.

	Hund's rules		Katt's rules
HI.	Saturate spin polarization - 011	KI.	Saturate spin-orbit polarization - 110
HII.	Optimize polarization 101	KII.	Optimize polarization 615(617)
	Induced polarizations:		Induced polarizations:
	110 and 112		415 and 505 (none)
HIII.	Let $\vec{w}^{110} < 0$	KIII.	Polarize 001, if possible

Table 5.2: *Katt's rules formulated for an f-electron shell, KII refers to an occupation $n \leq 6$, $(n > 6)$, i.e. polarization of the $f_{5/2}$ or $(f_{7/2})$ subshell. Hund's rules are presented for comparison to the weak spin-orbit regime. Populating the f-shell according to Hund's rules gives a result diagonal i l, m_l, s, m_s-basis, whereas populating the f-shell according to Katt's rules will give a density matrix close to diagonal in J, m_j-basis.*

5.3.3 VII: Multipolar ordering in actinide dioxides

In this paper we compare ground state properties of UO_2, NpO_2 and PuO_2 as calculated by the LDA+U method. These compounds show a varying degree of f-electron localization, UO_2 and NpO_2 are usually classified as semiconducting, whereas PuO_2 is an insulator. All compounds shows peculiarities in their magnetic properties. UO_2 is believed to have a $3\vec{k}$-AFM structure, NpO_2 shows signs of multipolar ordering and PuO_2 is nonmagnetic, in contrast with conventional LDA+U calculations, which predicts a magnetic ground state. We make a systematic investigation of all three compounds in terms of intra atomic multipolar ordering and interatomic ordering of the moments. We predict orderings in agreement with experiment for all compounds, where UO_2 is found to have two competing $3\vec{k}$ structures with similar energy. With the current numerics of the code we where unable to resolve whether the longitudinal or transverse ordering is the ground state. Both agree with measurements. NpO_2 also shows competing states with close to degenerate energy, one of the calculated solutions prohibits spin-moment by symmetry, indicating that this is likely to be the experimentally detected ground state. Lastly PuO_2 shows a $1\vec{k}$ arrangement of w_{-2}^{615} triakontadipoles, their moment integrates to zero, consistent with experimental observation.

### 5.3.4 VIII - X: Studies of triakontadipoles in Uranium based superconductors

The nature of the hidden order phase of URu_2Si_2 is still under heavy debate. A number of mechanisms have been proposed, for a recent review of experimental and theoretical work see Mydosh et. al [87]. Spurred by the appearance of the $\vec{w}^{615}$ multipoles appearing in many actinides we decided to investigate the properties of URu_2Si_2 using LDA+U and analyzing the results in terms of multipoles. Upon varying the screened Coulomb interaction we see a deviating behavior in the energy contribution of the $\vec{w}^{615}$ multipole. Already around $U \sim 1$ the energy contribution from $\vec{w}^{615}$ is dominant, and shows a sudden increase. Under pressure the system is known to undergo a phase transition from hidden order to AFM ordering. To investigate what happens to the system under pressure we calculated the energy contribution from all exchange channels for a number of volumes. The result is staggering, starting in the AFM phase, with a moment of $\sim 0.3\mu_B$ the contribution from the $\vec{w}^{615}$ tensor diverges for $a/a_0 \sim 1.015$, at the same we see a reversal of dipole moment at this point. This multipole breaks time reversal symmetry, and hence is detected by neutron diffraction even though the moment integrates to zero, for a graphical representation of a treakontadipole see Fig 5.1.

Calculations using LDA+DMFT indicates that a mixed hexadecapolar - dipolar phase should constitute the hidden order. The dipole giving rise to the small moment seen in experiments, and the hexadecapole to account for the "hidden" part [88]. Curious about the possibility of different kinds of multipolar ordering in this compound we performed systematic investigation all possible multipoles allowed by the experimental restrictions on symmetry. We identify a multipolar ordering which forbids dipolar ordering on the uranium site. The multipole is time-reversal odd, accounting for the tiny moment seen experiment.

The finding of the triakontadipoles in URu_2Si_2 inspired us to investigate the magnetic ordering of a few other Uranium based superconductors in the hexagonal structure, UPd_2Al_3, UNi_2Al_3 and UPt_3. These are so called heavy-fermion superconductors, that is, the effective mass of the electrons are orders of magnitude larger than that of a free electron. This implies poor conductivity, still they all enter a superconducting phase, coexisting with magnetic ordering.

5.3.5 XI: Multipolar ordering can explain the low spin-moment in LaFeAsO

The Fe based high Tc superconductors spurred an enormous interest upon discovery. Hope was naturally that another family of superconductors besides the cuperates wold shed light on the pairing mechanism. The mother compound, LaFeAsO, did not show signs of strong correlation in terms of mass enhancement, hence the first calculations where done with LDA. Alas, LDA produced
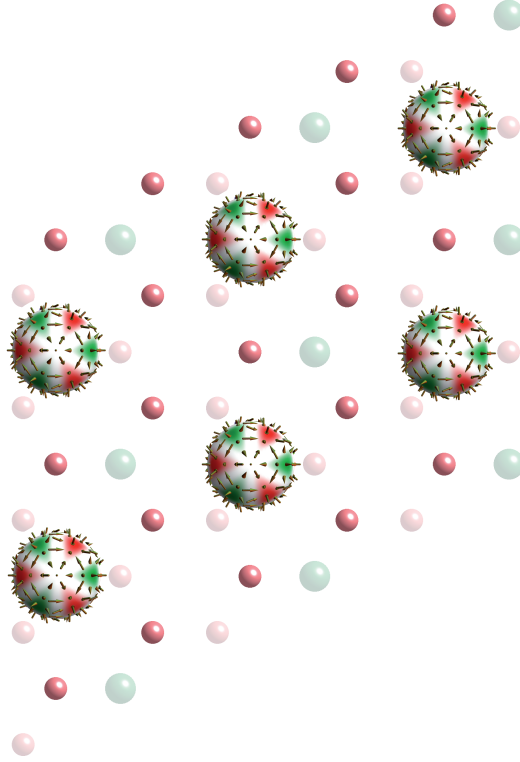
Figure 5.1: Triakontadipoles w_3^{615} arranged according to one of the competing solutions in UPt$_3$. Green represents magnetization density pointing outwards from the sphere, red represents inwards. Pt atoms are represented in red.Here the spheres represent the angular variation of the direction of the spin magnetization density for the triakontadipole w_3^{615}. The darker regions indicate where the spin axis is normal to the sphere, either outward (green) or inward (red). In both pictures the U atoms are pictured in green and Pd atoms in red. The shaded atoms are located on the subsequent layer. .

a magnetic moment almost 5 times as large as the experimentally detected one. Moreover, the *z*-component of the As position of not determined by symmetry, when it is relaxed using LDA the result is far from the experimental determined one. We show that adding on-site Coulomb interaction within the LDA+U scheme is enough to remedy all those problems. The results are analyzed in terms of the un-coupled multipoles due to the weak spin-orbit coupling in this system. From our calculations it is clear that the exchange energy chooses the w_{40}^{41} channel instead of the w_{00}^{01} channel that would produce a spin moment.

5.3.6 XII: Investigation of clustering an magnetism of Co dopants in ZnO

Spurred by the work of Dietl et. al, showing mean field estimates of Curie temperatures for various Mn doped p-type semiconductors above room temperature [89], the filed of dilute magnetic semiconductors was extremely active for many years [90, 91]. This study investigates clustering of Co in the wide band-gap semiconductor ZnO. Assessing the applicability of LDA and LDA+U we argue that LDA+U is the more appropriate of the two, based on the rather strong localization of Co d-orbitals. The magnetic interactions within the clusters are found to be weakly anti-ferromagnetic, particularly when applying LDA+U. Moreover we find strong tendency to form Co nano clusters, something detrimental to the use of this compound as a possible dilute magnetic semiconductor wether or not the clusters would have uncompensated ferromagnetic moments on the edges. Exchange interactions in wide band-gap semiconductors are short ranged, hence the formation of Co nano clusters will dilute the sample of possible percolation paths, putting us in super paramagnetic phase, regardless a small moment of the Co clusters. We also compute the orbital moment of a Co monomer on the Zn sublattice in the wurtzite structure, amounting to $0.14\mu_\mathrm{B}$ for $U = 5$eV and $J = 1$eV.

5.3.7 XIII: Investigations of the magnetic and electronic structure of SrRuO$_3$

The Ruddlesen-Popper series of Strontium Ruthenates show a spectacular range of intriguing magnetic properties. From computational as well as experimental point of view the results are quite inconclusive. The calculated magnetic moment varies between 1.09-2.0 [92, 93] when different methodology is applied. Hence we see the need for a thorough assessment of computational tools for this material. Recent work using LDA+DMFT shows an apparent spin-flip transition when U is increased ($J = U/2$) [94]. This is something we also see in e.g. Paper VIII and might be an implication that multipolar ordering might be of importance in this compound. In this initial study we see that the density of states compares reasonably well to experimental results. The mass-enhancement is also close to experimental results for $U \geq 2$eV, considering the range of the experimental numbers are 3.1 to 6.9 [95, 96]. Magnetic moment is also within the experimental range. Due to the large scatter of the experimental data it is difficult to judge which methods is appropriate. However, only the LDA+DMFT scheme yields a mass enhancement due to correlation effects, as there is a considerable experimental mass enhancement we conclude this methods is most suitable. The SPT-FLEX(G^HF should be more reliable for both magnetic and structural properties, with $U \sim 3$ as a reasonable estimate of the effective Coulomb interaction.

6. Magneto-crystalline anisotropies

Magnetic anisotropy is the result of the coupling between real space and spin space. It is generally divided into two different types, shape-anisotropy (SA) originating solely from magnetic dipole-dipole interaction and the magneto-crystalline anisotropy (MA) originating from both the spin-orbit interaction and the dipole-dipole interaction. In a thin film the SA is dominating and prefers a magnetization in the plane of the film, this is usually referred to as uniaxial anisotropy (or unidirectional under the influence of exchange bias). In highly symmetric crystals however, the SA is usually small compared to the MA, the MA is restricted by the symmetry of the crystal, for example cubic or hexagonal for homogeneous bulk materials. The MA is usually measured in terms of magneto-crystalline anisotropy energy (MAE), which is the energy it takes to flip the spin quantization axis from the most preferred one, the easy-axis, to another direction. From experimental point of view also interface anisotropy and magneto elastic anisotropy is commonly regarded as different phenomena then SA and MA, but from a computational perspective these effects are included as the reduce the symmetry of the computational cell. The energy contribution from interface and magneto elastic effects can of course be calculated, simply by comparing properties with bulk phases or unstrained structure.

In the field of spin-electronics the magnetization often acts as the information bearer. For example in a Magnetic Random Access Memory (MRAM) ferromagnetic films separated by some spacer material forms a unit with different resistance depending on the direction of the magnetization of the ferromagnetic films [97, 98]. Similarly, in hard-drives a solid disk with different domains of weakly coupled magnetic grains are used to store information. These applications put certain demands on the MAE. If the MAE is too small the information will be lost due to thermal fluctuations, if it is too high a very strong write field is needed. A higher MAE leads to the possibility of using smaller domains for data storage, hence a larger data density is achieved.

The MAE is generally parametrized in terms of the magnetization unit vectors in cartesian coordinates, or directional cosines in spherical coordinates. For a ferromagnetic grain of volume V_G we can define a magnetization unit vector

$$\overline{m} = \frac{\overline{M}}{M_s} = m_x \hat{x} + m_y \hat{y} + m_z \hat{z}, \tag{6.1}$$

where $\overline{M}$ is the total magnetization vector and M_s is the total spin-moment in V_G. It is now common to expand the MAE density in terms of m_i, due to time-reversal symmetry only even powers of m_i occurs.

For a uniaxial MAE we have a MAE density symmetric around one axis. Using the z-direction as reference, the deviation from m_z is the variable considered, i.e. $1 - m_z^2$ or $m_x^2 + m_y^2$ we can write the expansion as

$$G = K_0 + K_1(m_x^2 + m_y^2)^2 + K_2(m_x^2 + m_y^2)^4 + K_3(m_x^2 + m_y^2)^6 + K_4(m_x^2 + m_y^2)^8 + ...$$
(6.2)

Often spherical coordinates are used in the case of uniaxial anisotropy, giving $m_x^2 + m_y^2 = sin^2(\theta)$, θ being the polar angle. This leads to the simplified expression

$$G = K_0 + K_1(sin^2(\theta))^2 + K_2(sin^2(\theta))^4 + K_3(sin^2(\theta))^6 + K_4(sin^2(\theta))^8 + ...$$
(6.3)

Looking at the leading term, i.e. K_1 we see that we have two cases, one with a positive sign yielding a preferred direction along m_z, this type of uniaxial anisotropy is usually referred to as easy-axis anisotropy. The other case, a negative sign, gives a so called easy-plane anisotropy, i.e. the preferred direction is in the $m_x + m_y$ plane.

In a cubic symmetry the MAE density is expressed as

$$G = K_0 + K_1(m_x^2 m_y^2 + m_y^2 m_z^2 + m_z^2 m_x^2) + K_2 m_x^2 m_y^2 m_z^2 + ...$$
(6.4)

Again, looking at the leading term K_1 we see that a positive value yields a six-fold degeneracy with easy-axes along the unit vectors, whereas a negative value gives an eight-fold degeneracy where the unit vectors instead represent the hard axes.

The theoretical simulations are mainly focused at the MAE. The MAE is usually 10^{-6} to 10^{-3} eV per atom, hence only in the order of 10^{-10} to 10^{-6} of the total energy per atom. This puts very high demands on the numerical stability of the implementations, the full potential LMTO implementation in RSPt is well tested over the years, and the DMFT implementation is done in the same spirit, with great care of numerical stability.

In general the results coincide with experimental data, exceptions are primarily when materials with large structural relaxations (which can be taken into account, but are rather time consuming) or localized electron.

A strong MA is commonly desired in electronics applications where data is stored. The main reason for this to increase the data density in the storing device. An important property is then, of course, that the data is retained over some period of time. As described in the introduction the information on a magnetic hard-drive is stored in weakly coupled magnetic grains. The energy cost of flipping the magnetic moment of a grain is determined by its MAE. The stability of the magnetization in the grain can therefore be related to the total magnetic anisotropy energy of a grain, $K_u V$, where V is the volume of

the grain and K_u the uniaxial anisotropy constant. The energy of thermal fluctuations can be estimated though $k_B T$, where k_B is the Boltzmann constant and T is the temperature in Kelvin. For strong MA's the statistics of thermally induced magnetization reversals obeys an Arrhenius form [99], and the frequency of reversals can be estimated from

$$f \propto e^{-K_u V / k_B T}. \tag{6.5}$$

Hence, with a smaller ratio $K_u V / k_B T$ the probability of unwanted magnetization reversals increase [99]. As previously mentioned a too large MAE is not desired as a larger write field is required. This can be seen as H_W can be written as

$$H_W \propto K_U / M_s, \tag{6.6}$$

where M_s is the saturation magnetic moment [100].

Materials that exhibit strong MA are for example multi-layer structures and strained materials. The MA is proportional to the square of the spin-orbit coupling constant $\xi \propto \frac{1}{r}\frac{dV}{dr}$, which can reach very high values for heavy atoms. Therefore it is beneficial to alloy magnetic materials with heavy atoms. One of the most famous examples are FePt in the $L1_0$ structure. Pt is non magnetic with a large SO-constant, and Fe is magnetic with small SO-constant, the MAE between easy- and hard axes are only $\sim 1 \mu eV$. The FePt compound, however is extremely anisotropic with MAE ~ 3 meV [101], also strains can induce a very large MAE [100]. The effect can be viewed as an induced moment on the high SO-constant atoms, coupled to the magnetic atoms via the exchange coupling. Writing the energy difference induced by the SO-coupling as

$$\Delta E_{SO} = \sum_{qss'} \Delta E_q^{ss'} = \sum_{qss'} (E_q^{ss'}(\hat{n}_1) - (E_q^{ss'}(\hat{n}_2))), \tag{6.7}$$

where q is the atomic species, s, s' is occupied and unoccupied states, $\hat{n}_i$ is the spin-quantization axis. Using second order perturbation theory in SO coupling with an atom centered basis set the energy each of the $E_q^{ss'}(\hat{n})$ can be expressed as

$$\begin{aligned}
E_q^{ss'}(\hat{n}) = -\sum_{\mathbf{k}ij} \sum_{q'} \sum_{\{m\}} n_{\mathbf{k}is,qm,q'm'} n_{\mathbf{k}js',q'm'',qm'''} \\
\times \frac{\langle qms|H_{SO}(\hat{n})|qm'''s'\rangle \langle q'm''s'|H_{SO}(\hat{n})|q'm's\rangle}{\varepsilon_{\mathbf{k}j} - \varepsilon_{\mathbf{k}i}},
\end{aligned} \tag{6.8}$$

where $\mathbf{k}$ represents the sampling points in the Brillouin zone, i, j are the occupied and unoccupied states, q' is the sites in the unit cell and $\{m\} = \{m, m', m'', m'''\}$. The basis functions $|qlms\rangle$ are specified through the atomic site q, the l and m_s are the orbital and magnetic quantum numbers. For points in the Brillouin zone with both occupied and unoccupied states close to the

Fermi level $E_q^{ss'}(\hat{n}_i)$ will reach considerable size, as matrix elements in the nominator are non-zero, but the energy difference in the denominator approaches 0. This description is utilized in the publications described in the following section.

6.1 Summary of Papers XIV-XVI

In this section a brief introduction to the work related to magneto crystalline anisotropy is given.

## 6.1.1 XIV: A route to nano-laminates with high MAE

In this work we asses a possible route to create nano-laminates with very high magneto crystalline anisotropy energies. Today many of the hard magnetic materials are rare earth based, implying high price and fear for supply shortages [102], we suggest a nano-laminate composed of Fe and $W_x Re_{1-x}$, where $x = 0.6 - 0.8$. The method relies on strong hybridization between heavy ligands and lighter ferromagnetic materials. This induces a moment on the heavy ligands, coupled to the lattice with the strong spin-orbit coupling of the heavy element, cf. Eq. 6.8. To achieve a strong effect the coupled bands should be close to the Fermi-level, this indicates that we will have a large DOS close to the fermi level. This makes manufacturing intrinsically difficult, as the structure is less likely to be stable, however metastable compounds can now days be synthesized with standard lab technology. There is also a possibility of enhanced exchange coupling between the ferromagnet and the ligands, as a large DOS close to the Fermi-level can be reduced by the exchange splitting, similar to Stoner theory of ferromagnetism.

6.1.2 XV: Investigation of the magnetism and electronic structure of Fe_2P

A promising non-rare earth based compound with high MAE is Fe_2P, with the benefit of being composed of cheap and abundant elements. We focus on the impact of strain on MAE and magnetic moment, showing that the MAE is strongly affected by strain, while retaining a high magnetic moment. This indicates the possibility to use Fe_2P as a basis for further studies, where doping can be used to influence the c/a ratio. Heavier dopants could also act to increase the spin-orbit coupling constant, resulting in a higher MAE.

6.1.3 XVI: Impact of substrate surface reconstructions on the MAE of Fe on ZnSe

A thin layer of Fe on ZnSe is a prototypical ferromagnet-semiconductor interface structure, mainly due to the excellent lattice matching of the rotated bcc Fe lattice to the ZnSe zinc-blende structure. The magneto crystalline anisotropy was expected to show a uniaxial in-plane symmetry. The actual interface shows a quadratic symmetry, however, this is broken already in the second ZnSe layer below the surface. Initially the overlap between the ferromagnetic bcc Fe layers and the second semiconductor layer was argued to be negligible, however Sjöstedt *et. al* showed that this was not the case, and even an unrelaxed Fe surface on a sharp (1x1) ZnSe shows uniaxial behavior [103]. This study is a joint theoretical and experimental work, aiming to explain the strong reduction in the quadratic term K_2 in the expansion of magneto crystalline energy when comparing growth of Fe on a full coverage sharp (1x1) interface vs. a half coverage c(2x2) reconstructed interface. From theoretical perspective we modeled the structures using a sharp (1x1) interface (model *I*), a sharp c(2x2) interface (model *II*) and a c(2x2) interface with intermixed Fe atoms to the top Zn layer (model *III*) , see Fig. 6.1. The actual samples are assumed to contain all model structures to some extent due to interface defects, the (1x1) sample is likely to consist of mainly model *I*, and the c(2x2) sample mainly of model *II* and *III*. The atomic positions of the interfaces in all models are relaxed to their equilibrium positions. The calculations corroborates the experimental finding of the strong reduction of the K_2 anisotropy constant, the non-vanishing K_1 in the calculations of model *I* is ascribed to the hybridization between Fe and Se, together with a small buckling of the Fe atoms. The vanishing of K_1 in the experimental study of Fe on the sharp (1x1) ZnSe sample is not explained, but random distribution of interface defects and c(2x2) reconstructed domains with different orientations are possible reasons.
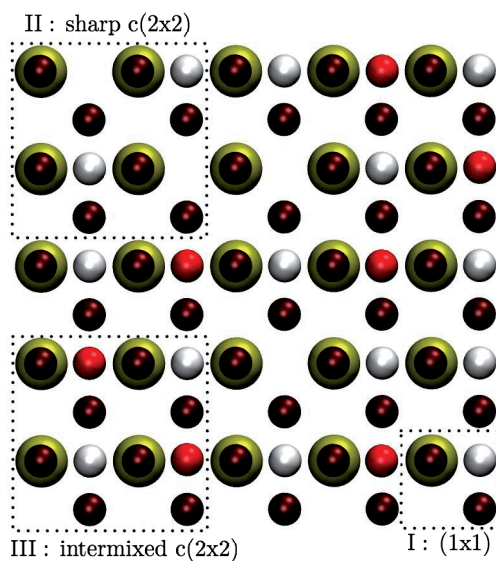
Figure 6.1: The figure shows a model interface for Fe deposited on Zn-terminated ZnSe. The yellow colored spheres represents Se atoms, the white Zn atoms, the light red intermixed Fe atoms and the dark red the first full coverage deposited Fe layer.

7. Perspectives and Outlook

Computational materials science is evolving very fast. Due to the increase in computer power we can now do in a matter of weeks what seemed impossible when I started my graduate studies. This enables more accurate methods to be implemented, but old implementations constantly have to be updated to make use of the latest hardware. The field of LDA+DMFT sees plenty of new fundamental developments in terms of basis sets for the correlated orbitals and impurity solvers whereas DFT already appears to be a standard method for first principles materials science.

The developments presented in this theses shows great promise for future use. Joining the LDA+DMFT scheme with spin-dynamics is a field likely to have a very beneficial outcome. DMFT provides temperature renormalization of the electronic structure and therefore also the interatomic interactions and the local magnetic moments. This leads to temperature dependent Heisenberg exchange parameters and likely a more realistic picture. The multipole analysis should be applied to more systems where the underlying reasons for magnetic anomalies are not known. It can also be used to extract generalized multipolar magnetic exchange parameters, extending the spin-dynamics scheme to include multipolar dynamics. The energy contributions from the DFT part of the calculation should also be analyzed on the same footing, so all energy contributions to the multipoles are available. This would provide an even more detailed knowledge of the intricate competitions between crystal field, spin-orbit coupling and exchange-correlation. The LDA+DMFT code would benefit from an in-house full U-matrix CT-QMC solver making use of the block diagonal and sparse representation of the many-body basis used in our Hubbard 1 and ED solvers. Constrained RPA to calculate the screened Coulomb interaction would also be a great addition to the code. The capability of running cluster DMFT calculations is already implemented, and should be tested and used. For long term development a full GW implementation should be considered, to provide correct band gap for band-insulators and parameter free GW+DMFT calculations. This would allow treatment of coupled quantum dots, doped semiconductors and most of all a fully parameter free method.

Acknowledgments

Before my start in Uppsala I was introduced to condensed matter theory during my masters thesis work in Linköping, where I was offered a project on alloy phase stability by Prof. Igor Abrikosov. That was good start and got me interested in the subject, mainly due to all nice discussions with Igor, Sergei, Björn and Andreas and the other guys. When it was time to apply for PhD positions I must really thank Till Burkert and Börje Johansson for an extra push in the Uppsala direction, without that I might have been to lazy to widen my views. Well in Uppsala I owe my greatest thanks to my main supervisor Lars Nordström, whom have always supported me over the years. Thank you also for endless patience with both theory, implementation and family life. I also want to thank Biplab Sanyal for tutoring and many nice discussions, we had many nice projects over the years! Without the support of Olle Eriksson I would've been stuck many times, you've supplied tons of nice projects and help on all kinds of subjects. As an endless source of both fun and information it's been great to work with you. To the dynamic duo Igor and Patrik, keep on betting, it makes theory more fun! Thank you also for all the help and discussions about everything, DMFT in particular. A big thanks to my fellow companions in the multipole project: the wizards of geometric shapes Francesco and Fredrik, without you the world would still be flat. I've also learned much from working with Sumanta on the MAE projects, always entertaining! Just as with Marcio, we should really get you stuff in the "trunk", so it doesn't go to waste once you finish (in California there's only surfing you know...). Without the work of Torbjörn the RSPt code would still be in stone-age shape (sorry John :)), the amount of testing and tidying up you've done deserves an award! We also had some great projects together, amazing what coffee table discussions can bring. A big thank you also goes to the rest of the RSPt development team, especially John for hosting me in Los Alamos a few times, but also Anna, Ann, Per and Meb, without you the code would die. My every day life is also enlightened very much by the lunch team the greek philosofer Petros, my personal trainer and humbler (in the physical sense) Henrik, Ingmar Bergman (Director of SD), connoisseur Jonas, freshman Kristoffer, soccer mom (literally) Annika, iron man Peter and Lisa the brewer, it's a good thing some people can still cook. Thanx also to the proofreading committee, Björn Alling, Torbjörn Björkman, Henrik Löfås, Sumanta Bhandary, Oleg Peil and of course my supervisors. Office mate Dmitry, you've already show me more equations than anyone else, thank's for keepin' it real! To all the oldies Lars

B, Anden, Micke, Cissi, Love, Diana, Johan, Ronny, Björn and the rest of you, you grew up way too fast :).

Many thanx also to the Ten Bar java group in Los Alamos, Travis, Nick, Anders, Matt and the rest of you. I've never experienced an office with a better barrista, or a more demanding set of customers for that matter.

The most of my gratitude I owe to my family, mom, dad, in-laws and so on. Especially Stina, I know this work has put at least as much pressure on you as it has on me. Ruben and Sixten, thank you for forcing me back to reality every day. With summer approaching I'll make sure we'll enjoy more time together!

Summary in Swedish:
Teoretiska studier av magnetism och elektronkorrelation i fasta material

Magnetism har länge använts av människan för en rad vitt skilda ändamål, t.ex. kompassen är nästan 1000 år gammal [1]. Idag ser vi direkta tillämpningsområden som datalagring, elektriska motorer, transformatorer och högtalare för att nämna några. Även indirekta effekter av magnetism kan vara väldigt viktiga, till exempel brukar ett material ha lägre densitet om det är magnetiskt än om det inte skulle vara det, något som har avgörande konsekvenser för t.ex. slutförvaring av kärnbränsle. Av dessa anledningar är det önskvärt att förstå de grundläggande mekanismerna bakom magnetismen, i förhoppning om att kunna förutsäga ett materials egenskaper och designa nya material med förbättrade egenskaper. I många fall är detta svårt eller dyrt att göra experimentellt. Därför är det önskvärt att simulera materialens egenskaper med hjälp av datorsimulationer. Materialen består av elektroner och atomkärnor, deras interaktioner beskrivs av Diracekvationen, vilken man alltså måste lösa med tillräcklig precision med hjälp av datorn. Just magnetism har visat sig synnerligen komplicerat ur denna aspekt. Anledningen är att magnetism ofta uppkommer på grund av att några av bindningselektronerna är starkt *korrelerade*, d.v.s. egenskaperna för en enskild elektron beror starkt på hur andra elektroner är positionerade. Det stora flertalet av bindningselektronerna är dock svagt korrelerade. Dessa behandlas väl av så kallad täthetsfunktionalteori, i vilken man ersätter växelverkan mellan individuella elektroner med växelverkan mellan enskilda elektroner och den laddningstäthet som övriga elektroner ger upphov till. För denna teori tilldelades dess grundare Walter Kohn Nobelpriset i Kemi 1998. Täthetsfunktionalteorin är exakt om utbytesväxelväxelverkan mellan elektronen och laddningstätheten är känd, vilket den inte är. Istället tillämpas approximativa *utbytesväxelverkansfunktionaler*, där man delvis tappar förmågan att beskriva de starkt korrelerade elektronerna som ger upphov till magnetismen. En stor del av denna avhandling handlar om utveckling och implementation av metoder för att behandla dom starkt korrelerade elektronerna med en explicit metod, d.v.s. där växelverkan mellan de starkt korrelerade elektronerna behandlas individuellt, medan dom elektroner som inte kräver den explicita behandlingen tas om hand med hjälp av täthetsfunktionalteorin. Den övergripande metoden kallas i detta fall för täthetsfunktionalteori + dynamisk medelfältsteori. Förutom beräkningsmetoder har mycket arbete lagts

på analysmetoder för resultaten, framförallt multipol analys av täthetsmatrisen och spektralfunktionen samt multipolernas energibidrag. Behovet av utförligare analys är uppenbart då man, för ett f-elektron skal, oftast analyserar endast 7 storheter av totalt 196: spin-moment $\vec{s}$, orbital-moment $\vec{l}$ samt laddning n. Den metod vi utvecklat erbjuder en komplett analys i termer av kopplade multipoler.

Vid sidan av metodutveckling har egenskaper hos ett flertal intressanta material undersökts med våra metoder. Här återfinns ett antal Uranbaserade okonventionella supraledare, URu_2Si_2, UPd_2Al_3, UNi_2Al_3 och UPt_3, för vilka mekanismen bakom supraledningen är okänd. Vi påvisar att en komplicerad intraatomär magnetisk struktur, s.k. triakontadipoler, (se t.ex. figur 5.1) är viktiga att ta hänsyn till i dessa material, något som är viktigt för den grundläggande förståelsen av dem. För högtemperatursupraledaren LaFeAsO visar vi hur en komplicerad magnetisk struktur ger en förklaringsmodell till en mängd fenomen som debatteras i forskningsfronten. Det visar sig att korrelationseffekter inte bara är viktiga för den magnetiska ordningen i materialet, utan även atomernas jämviktspositioner i kristallen. Vi har också undersökt δ-fasen av Plutonium. Den experimentellt uppmätta densiteten är långt under den förväntade för Pu i denna kristallstruktur. Tidigare beräkningar visade att den låga densiteten kunde bero på förekomsten av magnetism. Experimentellt har man senare visat att magnetism inte förekommer. Våra undersökningar indikerar spin-strömmar som en av de viktigaste orsakerna, tillsammans med en dynamisk skärmning av det magnetiska momentet, s.k. *Kondo effekt*. Ett stort antal material med starkt korrelerade elektroner samt stark spin-ban koppling har analyserats i termer av multipoler. Detta har lett fram till formuleringen av Katt's regler, en uppsättning regler för hur ett elektronskal polariseras då båda dessa kriterier är uppfyllda. Katt's regler är komplementära till Hund's regler för fria atomer. Det finns även förhoppning om att kunna använda elektronernas spin, istället för deras laddning, för att konstruera snabbare transistorer, s.k. *spintronik*. Detta förutsätter att man kan kontrollera både ledningsförmåga och magnetism i materialen. Tidigt hoppades man att isolatorer som t.ex. ZnO dopade med övergångsmetaller skulle ha just de sökta egenskaperna. Materialen är notoriskt svåra att syntetisera experimentellt, då dopatomerna lätt bildar kluster, och de magnetiska moment man sedermera mäter kan komma just från dessa kluster. Genom att simulera representativa kluster av Co atomer i ZnO visar vi att den magnetiska kopplingen är antiferromagnetisk, samt att atomerna tenderar att forma nano kluster, något som gör materialet olämpligt för spintronik-tillämpningar.

Ett annat viktigt fenomen för tillämpningar är *magnetokristallin anisotropi* (MA), d.v.s. att magnetismen har en prefererad riktning i kristallen. Utan denna skulle t.ex. magnetisk lagring av data vara omöjlig, transformatorerna skulle bara vara en bråkdel så effektiva etc. Material med hög MA innehåller ofta sällsynta jordartsmetaller. Tillgången på dessa är tidvis problematisk då

i princip hela produktionen sker i Kina. Vi har undersökt Fe_2P, ett lovande material med hög MA som bara består av billiga metaller, för att utröna de underliggande orsakerna till anisotropin i förhoppning om att i senare arbete designa nya funktionella material baserade på Fe_2P. Vi har också arbetat med att utveckla ett generellt tillvägagångssätt för att hitta nanolaminat med hög MA. Vi föreslår $5Fe/2W_{1-x}Re_x$, med $x = 0.6 - 0.8$. Enligt våra beräkningar är MA energitätheten i samma storleksordning som hos de bästa materialen baserade på sällsynta jordartsmetaller. Multilager av halvledarmaterial belagda med ferromagnetiska filmer är en annan viktig materialklass för datalagring. Här har vi, i samarbete med experiment, undersökt egenskaperna hos Fe belagt på ZnSe med olika typer av s.k. ytrekonstruktion. Här har vi ökat förståelsen för vad som bidrar till den starka uniaxiella anisotropin som ses i materialet. Det visar sig att avsaknaden av ytrekonstruktioner i ett av proven i princip släcker ut det uniaxiella bidraget, medan prov med c(2x2) rekonstruktion ger ett starkt bidrag. Figur 6.1 visar atomlagren närmast gränsskiktet mellan Fe och ZnSe och åskådliggör skillnaden mellan orekonstruerat (1x1), rekonstruerat c(2x2) och rekonstruerat med inblandning av Fe atomer i det översta Zn skiktet.

Avhandlingen är disponerad enligt följande: kapitel 1 är en något utförligare introduktion på engelska. Kapitel 2 ger en översikt till den grundläggande kvantmekanik som används i avhandlingen. Kapitel 3 tar upp de approximationer som görs för att kunna lösa Diracekvationen. Hur det implementeras tas upp i kapitel 4. Kapitel 5 tar upp multipolanalysen samt de resultat som den gett upphov till. Slutligen tas grunderna för beskrivningen av magnetokristallin anisotropi upp i kapitel 6.

Bibliography

[1] P. Mohn, "Magnetism in the solid state: an introduction," *Springer-Verlag Berlin*, 2003.

[2] N. Bohr, "Studier over metallernes elektrontheori ," *PhD Thesis*, 1911.

[3] H. Van Leeuwen, W. Mund, and M. Pauthenier, "Problèmes de la théorie électronique du magnétisme," *Journal de Physique et le Radium*, vol. 2, p. 361, 1921.

[4] K. Yoshida, "Theory of magnetism Springer series in solid-state sciences ," *Springer-Verlag Berlin*, 1998.

[5] J. Kübler, "Theory of itinerant electron magnetism," *Oxford science publications, Oxford*, 2000.

[6] M. Born and R. Oppenheimer, "Zur Quantentheorie der Moleküle," *Annalen der Physik*, vol. 84, pp. 457–484, 1927.

[7] F. Bloch, "Über die quantenmechanik der elektronen in kristallgittern," *Zeitschrift für Physik A Hadrons and Nuclei*, 1929.

[8] G. Floquet, "Sur les equations differentielles lineaires a coefficients periodiques," *Ann. Ecole Norm. Ser*, vol. 12, pp. 47–88, 1883.

[9] D. Koelling and B. Harmon, "A technique for relativistic spin-polarised calculations," *J Phys C Solid State*, vol. 10, p. 3107, 1977.

[10] J. C. Slater, "The Theory of Complex Spectra," *Physical Review*, vol. 34, pp. 1293–1322, Nov. 1929.

[11] R. Dreizler and E. Gross, "Density functional theory: an approach to the quantum many-body problem ," *Springer-Verlag Berlin*, 1990.

[12] K. Capelle, "A bird's-eye view of density-functional theory," *arXiv*, vol. cond-mat.mtrl-sci, Nov. 2002.

[13] K. Burke, "The ABC of DFT," *http://dft.uci.edu/book/gamma/*, 2007.

[14] P. Hohenberg and W. Kohn, "Inhomogeneous electron gas," *Physical Review B*, vol. 136, no. 3B, pp. B864–&, 1964.

[15] M. Levy, "Universal Variational Functionals of Electron Densities, First-Order Density Matrices, and Natural spin-orbitals and solutions of the v-representability problem," *PNAS*, vol. 76, no. 12, p. 6062, 1979.

[16] M. Levy, "ELECTRON-DENSITIES IN SEARCH OF HAMILTONIANS," *Phys Rev A*, vol. 26, no. 3, pp. 1200–1208, 1982.

[17] W. Kohn and L. Sham, "Self-consistent equations including exchange and correlation effects," *Physical Review*, vol. 140, no. 4A, pp. 1133–&, 1965.

[18] U. Barth and L. Hedin, "Local Exchange-Correlation Potential for Spin Polarized Case," *J Phys C Solid State*, vol. 5, no. 13, pp. 1629–&, 1972.

[19] D. Ceperley and B. Alder, "Ground State of the Electron Gas by a Stochastic Method," *Phys Rev Lett*, vol. 45, no. 7, p. 566, 1980.

[20] S. Vosko, L. Wilk, and M. Nusair, "Accurate Spin-Dependent Electron Liquid Correlation Energies for Local Spin-Density Calculations - a Critical Analysis," *Canadian Journal of Physics*, vol. 58, no. 8, pp. 1200–1211, 1980.

[21] J. Perdew and A. ZUNGER, "Self-interaction correction to density-functional approximations for many-electron systems," *Physical Review B*, 1981.

[22] J. Perdew, K. Burke, and M. Ernzerhof, "Generalized Gradient Approximation Made Simple," *Phys Rev Lett*, vol. 77, no. 18, p. 3865, 1996.

[23] J. Perdew, A. Ruzsinszky, G. Csonka, and O. Vydrov, "Restoring the Density-Gradient Expansion for Exchange in Solids and Surfaces," *Phys Rev Lett*, vol. 100, p. 136406, 2008.

[24] R. Armiento and A. Mattsson, "Functional designed to include surface effects in self-consistent density functional theory," *Physical Review B*, vol. 72, p. 085108, 2005.

[25] V. Anisimov, J. Zaanen, and O. Andersen, "Band theory and Mott insulators: Hubbard U instead of Stoner I," *Physical Review B*, 1991.

[26] O. Gunnarsson, "Calculation of parameters in model Hamiltonians," *Physical Review B*, vol. 41, no. 1, p. 514, 1990.

[27] V. Anisimov and O. Gunnarsson, "Density-functional calculation of effective Coulomb interactions in metals," *Physical Review B*, vol. 43, no. 10, p. 7570, 1991.

[28] F. Aryasetiawan, K. Karlsson, O. Jepsen, and U. Schonberger, "Calculations of Hubbard U from first-principles," *Physical Review B*, vol. 74, no. 12, p. 125106, 2006.

[29] P. W. Anderson, "Localized Magnetic States in Metals," *Physical Review*, vol. 124, no. 1, pp. 41–&, 1961.

[30] W. Metzner and D. Vollhardt, "Correlated Lattice Fermions in d=inf Dimensions," *Phys Rev Lett*, vol. 62, pp. 324–327, Jan. 1989.

[31] A. Georges and G. Kotliar, "Hubbard model in infinite dimensions," *Physical Review B*, vol. 45, no. 12, p. 6479, 1992.

[32] V. Anisimov, A. Poteryaev, M. Korotin, A. Anokhin, and G. Kotliar, "First-principles calculations of the electronic structure and spectra of strongly correlated systems: dynamical mean-field theory," *J Phys-Condens Mat*, vol. 9, no. 35, pp. 7359–7367, 1997.

[33] A. Lichtenstein and M. Katsnelson, "Ab initio calculations of quasiparticle band structure in correlated systems: LDA++ approach," *Physical Review B*, vol. 57, no. 12, p. 6884, 1998.

[34] A. Georges, G. Kotliar, W. Krauth, and M. Rozenberg, "Dynamical mean-field theory of strongly correlated fermion systems and the limit of infinite dimensions," *Rev Mod Phys*, vol. 68, no. 1, pp. 13–125, 1996.

[35] G. Kotliar, S. Y. Savrasov, K. Haule, V. S. Oudovenko, O. Parcollet, and C. A. Marianetti, "Electronic structure calculations with dynamical mean-field theory," *Rev Mod Phys*, vol. 78, pp. 865–951, Aug. 2006.

[36] A. Georges, "Strongly Correlated Electron Materials: Dynamical Mean-Field Theory and Electronic Structure," *arXiv*, vol. cond-mat.str-el, Mar. 2004.

[37] T. Maier, M. Jarrell, T. Pruschke, and M. Hettler, "Quantum cluster theories," *Rev Mod Phys*, vol. 77, p. 1027, 2005.

[38] K. Held, "Electronic structure calculations using dynamical mean field theory," *Advances in Physics*, vol. 56, no. 6, pp. 829–926, 2007.

[39] J. Hirsch and R. Fye, "Monte Carlo Method for Magnetic Impurities in Metals," *Phys Rev Lett*, vol. 56, pp. 2521–2524, June 1986.

[40] M. Jarrell, "Hubbard-Model in Infinite Dimensions - a Quantum Monte-Carlo Study," *Phys Rev Lett*, vol. 69, no. 1, pp. 168–171, 1992.

[41] E. Gull, A. Millis, A. Lichtenstein, A. Rubtsov, M. Troyer, and P. Werner, "Continuous-time Monte Carlo methods for quantum impurity models," *Rev Mod Phys*, vol. 83, pp. 349–404, May 2011.

[42] N. Bickers, D. Scalapino, and S. White, "Conserving Approximations for Strongly Correlated Electron Systems: Bethe-Salpeter Equation and Dynamics for Two-Dimensional Hubbard Model," *Phys Rev Lett*, vol. 62, no. 8, p. 961, 1989.

[43] M. Katsnelson and A. Lichtenstein, "First-principles calculations of magnetic interactions in correlated systems," *Physical Review B*, vol. 61, no. 13, p. 8906, 2000.

[44] L. Pourovskii, M. Katsnelson, and A. Lichtenstein, "Correlation effects in electronic structure of actinide monochalcogenides," *Physical Review B*, vol. 72, no. 11, p. 115106, 2005.

[45] L. V. Pourovskii, M. Katsnelson, A. Lichtenstein, L. Havela, T. Gouder, F. Wastin, A. B. Shick, V. Drchal, and G. H. Lander, "Nature of non-magnetic strongly-correlated state in delta-plutonium," *Europhys Lett*, vol. 74, no. 3, p. 479, 2006.

[46] L. Pourovskii, G. Kotliar, M. I. Katsnelson, and A. I. Lichtenstein, "Dynamical mean-field theory investigation of specific heat and electronic structure of alpha- and delta-Plutonium," *Physical Review B*, vol. 75, no. 23, p. 235107, 2007.

[47] M.-T. Suzuki and P. Oppeneer, "Dynamical mean-field theory of a correlated gap formation in plutonium monochalcogenides," *Physical Review B*, vol. 80, p. 161103, Oct. 2009.

[48] G. Baym and L. Kadanoff, "Conservation Laws and Correlation Functions," *Physical Review*, vol. 124, no. 2, pp. 287–&, 1961.

[49] V. Drchal, V. Janis, J. Kudrnovsky, V. Oudovenko, X. Dai, K. Haule, and G. Kotliar, "Dynamical correlations in multiorbital Hubbard models: fluctuation exchange approximations," *J Phys-Condens Mat*, vol. 17, no. 1, pp. 61–74, 2005.

[50] I. V. Solovyev, "Orbital Polarization in Itinerant Magnets," *Phys Rev Lett*, vol. 95, p. 4, Dec. 2005.

[51] S. Chadov, J. Minár, M. I. Katsnelson, H. Ebert, D. Ködderitzsch, and A. I. Lichtenstein, "Orbital magnetism in transition metal systems: The role of local correlation effects," *Europhys Lett*, vol. 82, p. 37001, Apr. 2008.

[52] P. Thunstrom, I. Di Marco, A. Grechnev, S. Lebegue, M. I. Katsnelson, A. Svane, and O. Eriksson, "Multiplet effects in the electronic structure of intermediate-valence compounds," *Physical Review B*, vol. 79, no. 16, p. 165104, 2009.

[53] K. Haule, S. Kirchner, J. Kroha, and P. Wölfle, "Anderson impurity model at finite Coulomb interaction U: Generalized noncrossing approximation," *Physical Review B*, vol. 64, Sept. 2001.

[54] H. Hafermann, C. Jung, S. Brener, M. I. Katsnelson, A. N. Rubtsov, and A. I. Lichtenstein, "Superperturbation solver for quantum impurity models," *Epl-Europhys Lett*, vol. 85, no. 2, pp. –, 2009.

[55] S. Biermann, F. Aryasetiawan, and A. Georges, "First-principles approach to the electronic structure of strongly correlated systems: Combining the GW approximation and dynamical mean-field theory," *Phys Rev Lett*, vol. 90, no. 8, pp. –, 2003.

[56] M. Czyżyk and G. Sawatzky, "Local-density functional and on-site correlations: The electronic structure of La_ 2 CuO_ 4 and . . . ," *Physical Review B*, 1994.

[57] A. Petukhov, I. Mazin, L. Chioncel, and A. Lichtenstein, "Correlated metals and the LDA+ U method," *Physical Review B*, vol. 67, no. 15, p. 153106, 2003.

[58] A. Lichtenstein, M. Katsnelson, and G. Kotliar, "Finite-Temperature Magnetism of Transition Metals: An ab initio Dynamical Mean-Field Theory," *Phys Rev Lett*, 2001.

[59] J. Braun, J. Minaer, H. Ebert, M. I. Katsnelson, and A. I. Lichtenstein, "Spectral function of ferromagnetic 3d metals: A self-consistent LSDA+DMFT approach combined with the one-step model of photoemission," *Phys Rev Lett*, vol. 97, no. 22, p. 227601, 2006.

[60] O. Andersen, "Linear Methods in Band Theory," *Physical Review B*, vol. 12, no. 8, pp. 3060–3083, 1975.

[61] H. L Skriver, "The LMTO method," *Springer-Verlag Berlin*, p. 281, 1984.

[62] J. M. Wills, M. Alouani, P. Andersson, A. Delin, O. Eriksson, and O. Grechnev, "Full-Potential Electronic Structure Method," *Springer Series in Solid-State Sciences*, pp. 1–195, Aug. 2010.

[63] http://www.rspt.net.

[64] J. Slater, "Wave functions in a periodic potential," *Physical Review*, vol. 51, p. 846, 1937.

[65] D. Singh and L. Nordström, "Planewaves, Pseudopotentials, and the LAPW method," *Springer Verlag*, 2006.

[66] R. Martin, "Electronic structure," *Cambridge university press, Cambridge*, 2004.

[67] http://elk.sourceforge.net.

[68] K. Haule, C.-H. Yee, and K. Kim, "Dynamical mean-field theory within the full-potential methods: Electronic structure of CeIrIn_5 , CeCoIn_5 , and CeRhIn_5," *Physical Review B*, vol. 81, p. 195107, May 2010.

[69] S. Savrasov and G. Kotliar, "Spectral density functionals for electronic structure calculations," *Physical Review B*, vol. 69, no. 24, p. 245101, 2004.

[70] L. V. Pourovskii, B. Amadon, S. Biermann, and A. Georges, "Self-consistency over the charge density in dynamical mean-field theory: A linear muffin-tin implementation and some physical implications," *Physical Review B*, vol. 76, no. 23, pp. –, 2007.

[71] E. Condon and E. Condon, "The Theory of Atomic Spectra." The university press, Cambridge, 1935.

[72] A. L Fetter and J. Dirk Walecka, "Quantum Theory of Many-Particle Systems," *McGraw-Hill book company*, p. 617, 2003.

[73] I. Di Marco, J. Minar, S. Chadov, M. I. Katsnelson, H. Ebert, and A. I. Lichtenstein, "Correlation effects in the total energy, the bulk modulus, and the lattice constant of a transition metal: Combined local-density approximation and dynamical mean-field theory applied to Ni and Mn," *Physical Review B*, vol. 79, no. 11, p. 115111, 2009.

[74] V. Galitskii and Migdal, AB, "Application of Quantum Field Theory Methods to the Many Body Problem," *Sov Phys Jetp-Ussr*, vol. 7, no. 1, pp. 96–104, 1958.

[75] N. Mermin, "Thermal Properties of Inhomogeneous Electron Gas," *Physical Review*, vol. 137, p. A1441, 1965.

[76] M. Methfessel and A. Paxton, "High-Precision Sampling for Brillouin-Zone Integration in Metals," *Physical Review B*, vol. 40, pp. 3616–3621, 1989.

[77] N. Marzari, D. Vanderbilt, A. De Vita, and M. Payne, "Thermal contraction and disordering of the Al (110) surface," *Phys Rev Lett*, vol. 82, no. 16, pp. 3296–3299, 1999.

[78] O. Jepsen and O. Andersen, "Electronic Structure of Hcp Ytterbium," *Solid State Commun*, vol. 9, no. 20, pp. 1763–+, 1971.

[79] P. E. Blochl, O. Jepsen, and O. Andersen, "Improved Tetrahedron Method for Brillouin-Zone Integrations," *Physical Review B*, vol. 49, pp. 16223–16233, 1994.

[80] S. Froyen, "Brillouin-Zone Integration by Fourier Quadrature - Special Points for Superlattice and Supercell Calculations," *Physical Review B*, vol. 39, pp. 3168–3172, 1989.

[81] P. Santini, S. Carretta, G. Amoretti, and R. Caciuffo, "Multipolar interactions in f-electron systems: The paradigm of actinide dioxides," *Rev Mod Phys*, 2009.

[82] G. van der Laan, "Angular momentum sum rules for x-ray absorption," *Physical Review B*, vol. 57, no. 1, pp. 112–115, 1998.

[83] F. Cricchio, F. Bultmark, and L. Nordström, "Exchange energy dominated by large orbital spin-currents in delta-Pu," *Physical Review B*, vol. 78, p. 100404, Sept. 2008.

[84] K. Moore, G. van der Laan, R. Haire, M. Wall, and A. Schwartz, "Oxidation and aging in U and Pu probed by spin-orbit sum rule analysis: Indications for covalent metal-oxide bonds," *Physical Review B*, vol. 73, no. 3, pp. –, 2006.

[85] J. H. Shim, K. Haule, and G. Kotliar, "X-ray absorption branching ratio in actinides: LDA plus DMFT approach," *Europhys Lett*, vol. 85, no. 1, p. 17007, 2009.

[86] J. H. Shim, K. Haule, S. Savrasov, and G. Kotliar, "Screening of magnetic moments in PuAm alloy: Local density approximation and dynamical mean field theory study," *Phys Rev Lett*, vol. 101, no. 12, pp. –, 2008.

[87] J. Mydosh and P. Oppeneer, "Colloquium: Hidden order, superconductivity, and magnetism: The unsolved case of URu_2Si_2," *Rev Mod Phys*, vol. 83, pp. 1301–1322, Nov. 2011.

[88] K. Haule and G. Kotliar, "Arrested Kondo effect and hidden order in URu2Si2," *Nature Physics*, Sept. 2009.

[89] T. Dietl, H. Ohno, F. Matsukura, J. Cibert, and D. Ferrand, "Zener model description of ferromagnetism in zinc-blende magnetic semiconductors," *Science*, vol. 287, no. 5455, pp. 1019–1022, 2000.

[90] T. Jungwirth, J. Mašek, J. Kučera, and A. H. MacDonald, "Theory of ferromagnetic (III,Mn)V semiconductors," *Rev Mod Phys*, vol. 78, pp. 809–864, Aug. 2006.

[91] K. Sato, L. Bergqvist, J. Kudrnovsky, P. H. Dederichs, O. Eriksson, I. Turek, B. Sanyal, G. Bouzerar, H. Katayama-Yoshida, V. A. Dinh, T. Fukushima, H. Kizaki, and R. Zeller, "First-principles theory of dilute magnetic semiconductors," *Rev Mod Phys*, vol. 82, no. 2, pp. 1633–1690, 2010.

[92] J. Rondinelli, N. Caffrey, S. Sanvito, and N. Spaldin, "Electronic properties of bulk and thin film SrRuO3: Search for the metal-insulator transition," *Physical Review B*, vol. 78, p. 155107, Oct. 2008.

[93] H.-T. Jeng, S.-H. Lin, and C.-S. Hsue, "Orbital Ordering and Jahn-Teller Distortion in Perovskite Ruthenate SrRuO3," *Phys Rev Lett*, vol. 97, Aug. 2006.

[94] E. Jakobi, S. Kanungo, S. Sarkar, S. Schmitt, and T. Saha-Dasgupta, "LDA plus DMFT study of Ru-based perovskite SrRuO3 and CaRuO3," *Physical Review B*, vol. 83, no. 4, pp. –, 2011.

[95] J. Ahn, J. Bak, H. Choi, T. Noh, J. Han, Y. Bang, J. Cho, and Q. Jia, "Spectral Evolution in (Ca,Sr)RuO3 near the Mott-Hubbard Transition," *Phys Rev Lett*, vol. 82, pp. 5321–5324, June 1999.

[96] C. Alexander, S. McCall, P. Schlottmann, J. Crow, and G. Cao, "Angle-resolved de Haas–van Alphen study of SrRuO3," *Physical Review B*, vol. 72, July 2005.

[97] M. Baibich, J. Broto, A. Fert, and F. Van Dau, "Giant Magnetoresistance of (001) Fe/(001) Cr Magnetic Superlattices," *Phys Rev Lett*, 1988.

[98] G. Binasch, P. Grünberg, F. Saurenbach, and W. Zinn, "Enhanced magnetoresistance in layered magnetic structures with antiferromagnetic interlayer exchange," *Physical Review B*, 1989.

[99] J. García-Palacios and F. Lázaro, "Langevin-dynamics study of the dynamical properties of small magnetic particles," *Physical Review B*, 1998.

[100] T. Burkert, O. Eriksson, S. Simak, A. Ruban, B. Sanyal, L. Nordström, and J. Wills, "Magnetic anisotropy of L1(0) FePt and Fe1-xMnxPt," *Physical Review B*, vol. 71, pp. –, 2005.

[101] P. Ravindran, A. Kjekshus, H. Fjellvåg, and P. James, "Large magnetocrystalline anisotropy in bilayer transition metal phases from first-principles full-...," *Physical Review B*, 2001.

[102] D. Kramer, "Concern grows over China's dominance of rare-earth metals," *Phys. Today*, vol. 63, no. 5, p. 22, 2010.

[103] E. Sjöstedt, L. Nordström, F. Gustavsson, and O. Eriksson, "Uniaxial magnetocrystalline anisotropy of metal/semiconductor interfaces: Fe/ZnSe(001)," *Phys Rev Lett*, vol. 89, pp. –, 2002.

[104] V. Anisimov, F. Aryasetiawan, and A. Lichtenstein, "First-principles calculations of the electronic structure and spectra of strongly correlated systems: The LDA+U method," *J Phys-Condens Mat*, vol. 9, no. 4, pp. 767–808, 1997.

[105] G.-Q. Liu, V. N. Antonov, O. Jepsen, and O. K. Andersen, "Coulomb-Enhanced Spin-Orbit Splitting: The Missing Piece in the Sr_2RhO_4 Puzzle," *Phys Rev Lett*, vol. 101, July 2008.

[106] T. Palstra, A. Menovsky, J. Vandenberg, A. Dirkmaat, P. Kes, G. Nieuwenhuys, and J. Mudosh, "Superconducting and Magnetic Transitions in the Heavy-Fermion System URu2Si2," *Phys Rev Lett*, vol. 55, no. 24, pp. 2727–2730, 1985.

[107] S. Savrasov and G. Kotliar, "Ground State Theory of delta-Pu," *Phys Rev Lett*, vol. 84, pp. 3670–3673, Apr. 2000.

[108] M. van Schilfgaarde, I. Abrikosov, and B. Johansson, "Origin of the Invar effect in iron-nickel alloys," *Nature*, vol. 400, no. 6739, pp. 46–49, 1999.

[109] I. V. Solovyev, P. H. Dedrichs, and I. Mertig, "Origin of orbital magnetization and magnetocrystalline anisotropy in TX ordered alloys (where T=Fe,Co and X=Pd,Pt)," *Physical Review B*, vol. 52, p. 13419, June 2008.

[110] I. V. Solovyev and M. Imada, "Screening of Coulomb interactions in transition metals," *Physical Review B*, vol. 71, no. 4, p. 11, 2005.

[111] I. Solovyev, A. Liechtenstein, and K. Terakura, "Is Hund's second rule responsible for the orbital magnetism in solids?," *Phys Rev Lett*, vol. 80, no. 26, pp. 5758–5761, 1998.

[112] I. Solovyev, P. Dederichs, and V. Anisimov, "Correlated atomic limit in the local-density approximation and the electronic structure of d impurities in Rb," *Physical Review B*, 1994.

Acta Universitatis Upsaliensis

Digital Comprehensive Summaries of Uppsala Dissertations from the Faculty of Science and Technology 920

Editor: The Dean of the Faculty of Science and Technology

A doctoral dissertation from the Faculty of Science and Technology, Uppsala University, is usually a summary of a number of papers. A few copies of the complete dissertation are kept at major Swedish research libraries, while the summary alone is distributed internationally through the series Digital Comprehensive Summaries of Uppsala Dissertations from the Faculty of Science and Technology.